JACS Au
AN OPEN ACCESS JOURNAL OF THE AMERICAN CHEMICAL SOCIETY

pubs.acs.org/jacsau

Perspective

Trends in Photopolymerizable Bioinks for 3D Bioprinting of Tumor Models

Sriram Bharath Gugulothu, Sonal Asthana, Shervanthi Homer-Vanniasinkam, and Kaushik Chatterjee*

Cite This: *JACS Au* 2023, 3, 2086−2106

Read Online

ACCESS | Metrics & More | Article Recommendations

ABSTRACT: Three-dimensional (3D) bioprinting technologies involving photopolymerizable bioinks (PBs) have attracted enormous attention in recent times owing to their ability to recreate complex structures with high resolution, mechanical stability, and favorable printing conditions that are suited for encapsulating cells. 3D bioprinted tissue constructs involving PBs can offer better insights into the tumor microenvironment and offer platforms for drug screening to advance cancer research. These bioinks enable the incorporation of physiologically relevant cell densities, tissue-mimetic stiffness, and vascularized channels and biochemical gradients in the 3D tumor models, unlike conventional two-dimensional (2D) cultures or other 3D scaffold fabrication technologies. In this perspective, we present the emerging techniques of 3D bioprinting using PBs in the context of cancer research, with a specific focus on the efforts to recapitulate the complexity of the tumor microenvironment. We describe printing approaches and various PB formulations compatible with these techniques along with recent attempts to bioprint 3D tumor models for studying migration and metastasis, cell−cell interactions, cell−extracellular matrix interactions, and drug screening relevant to cancer. We discuss the limitations and identify unexplored opportunities in this field for clinical and commercial translation of these emerging technologies.

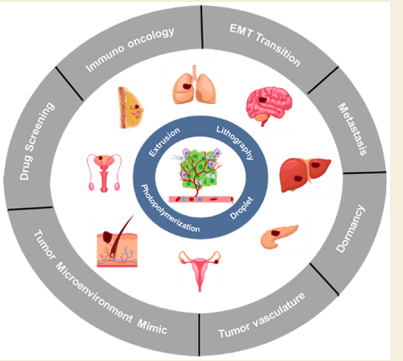

KEYWORDS: *Polymers, Cancer, Tissue engineering, Drug screening, Additive manufacturing*

1. INTRODUCTION

Malignant tumors can be considered as small organs comprising several stromal and malignant cells associated with a hypoxic core, leaky vasculature, altered matrix metalloproteinase (MMP) expression, and increased stiffness of extracellular matrix (ECM) in contrast to normal tissues.[1] *In vitro* platforms, *in vivo* (animal) models such as syngeneic,[2] ectopic,[3] and orthotopic[4] models involving patient-derived xenografts (PDX), and computational models have been crucial in developing a better understanding of molecular mechanisms underlying tumor biology and efficient diagnostics and therapeutics for patient care.[5] However, the drawbacks of current xenograft and syngeneic mouse models for screening cancer therapeutics are widely recognized. Particularly, the inability of these models to accurately replicate the immunological and stromal elements of the human tumor microenvironment results in 95% failure of the translation of cancer therapeutics from preclinical to clinical stages. These limitations underscore the importance of developing scalable human relevant *in vitro* tumor models for high throughput screening for expedited and affordable drug discovery and potential use for personalized medicine. The multicellular interactions, spatial localizations, and varied ECM stiffness in the tumor microenvironment (TME) are difficult to recapitulate using conventional techniques such as two-dimensional (2D) cell culture.[6] Three-dimensional (3D) *in vitro* models are being increasingly explored to provide a more clinically relevant tumor model than 2D culture.[7] 3D platforms comprising spheroid cultures,[8] scaffold-based models,[9] and organ-on-a-chip[10,11] offer various advantages to overcome some of the limitations of 2D cultures. Nevertheless, these techniques continue to be limited by their inability to efficiently recreate the full complexity of the TME with respect to spatial localization, vasculature, and architectural and dynamic complexity.[12]

The rapid advancement in additive manufacturing (AM) affords the layer-by-layer fabrication of complex parts from 3D virtual models. Depending on the method used to create the layers for a 3D part, additive manufacturing processes have been classified into seven categories by the American Society for Testing and Materials (ASTM), such as photopolymerization, material extrusion, material jetting, powder bed fusion, binder jetting, sheet lamination, and direct energy deposition.[13] Even though 3D printed scaffolds can mimic complex geometries,[14] these are limited by the lack of homogeneous cell

Received: June 1, 2023
Revised: July 25, 2023
Accepted: July 26, 2023
Published: August 11, 2023

seeding and large volume occupancy by the scaffold itself, which limits their utility to recreate the multicellular spatial localization of cells in the tumor microenvironment. As 3D bioprinting techniques are increasingly adopted for fabricating tissue scaffolds, it has become feasible to fabricate complex constructs and spatially pattern cells in scaffolds to recapitulate the organization of tissues *in vivo*.[15,16] Several studies have shown that multicellular and ECM mimetic bioink-based 3D bioprinted constructs can recreate *in vivo* specific neoplastic tissues and provide a tunable system for understanding multiple tumorigenic events in different TMEs.[12,17,18]

Bioinks constitute a key component of bioprinting technology by not only enabling the efficient and rapid fabrication of the designed part with high precision and accuracy but also providing biochemical, mechanical, and geometrical cues for cellular proliferation, differentiation, and organization. Notably, tissue scaffolds can be prepared from biomaterial inks or bioinks. Biomaterial inks can be prepared from natural, synthetic, or semisynthetic biomaterials, which are cytocompatible and must be suited for the printing technique applied to realize a complex 3D geometry for the intended applications.[19] The cells are introduced after the fabrication of the scaffold prepared from the biomaterial inks.[20] Bioinks refer to biomaterial ink formulations that support 3D printing in the presence of live cells. However, for ease of discussion and underlying similarities, we discuss both of these categories of ink formulations and refer to them as bioinks. The inks may be cross-linked, either physically or chemically, either during 3D printing or postprinting to augment the stability and maintenance of the constructs for downstream applications. Noncovalent approaches such as ionic cross-linking, thermoresponsive gelation, and DNA hybridization, and covalent approaches, such as enzymatic cross-linking, Schiff base reactions, and photopolymerization-based curing, are widely adapted to provide mechanical stability to 3D bioprinted constructs. Bioinks can be composed of either nonphotocurable or photocurable components or a mix of both depending upon the printing approach and targeted application. Cross-linking methods for inks that are not photopolymerizable primarily involve noncovalent interactions leading to soft constructs with limited mechanical stability. The utility of these bioinks can be limited by their requirement for specific buffer conditions and temperatures depending upon the polymer and functional groups involved in noncovalent interactions. Enzymatic cross-linking approaches can be limited by slow reactions and the necessary reaction conditions.[21]

Photopolymerizable bioinks (PBs) represent a major class of bioinks, constituting light-sensitive polymers that are polymerized by a photoinitiator (PI) and may optionally contain other additives such as rheological modifiers and photoabsorbers. These bioinks are widely explored through extrusion, droplet (jetting), and vat-based bioprinting modalities[22] for various applications such as tissue engineering, drug delivery, and 3D cell encapsulation. PBs offer several advantages compared to nonphotopolymerizable bioinks. Biochemical and mechanical gradients can be established in the 3D bioprinted constructs to recreate tumor and tissue-level anisotropy.[23] Specifically, in vat-based bioprinting, PBs can provide better resolutions and precision than extrusion-based bioinks to realize the complex tumor microarchitectures such as leaky vasculature, lobular structures, and glandular geometries to mimic several complex organotypic microphysiology.[24] The utility of PBs in vat-based bioprinting involving biomaterials such as alginate,[25] gelatin, and hyaluronic acid can avoid filler materials such as rheological modifiers needed in extrusion-based bioprinting to render them printable and minimize undesired cellular response.[26] We and others have introduced novel and improved polymeric bioink formulations for vat-based bioprinting for various tissue engineering applications.[27−29] Even though certain limitations exist, such as cellular-level toxicity due to exposure to far ultraviolet (UV) light and free radicals produced by PI and unreacted polymers, exist. These can be minimized by using optimal concentrations of the polymers and PIs with visible light sensitivity to avoid genetic alterations.[30]

Vat-based 3D bioprinting techniques, such as stereolithography (SLA), digital light processing (DLP), and two-photon polymerization (2PP),[31] have evolved to enable the incorporation of several cell types in 3D scaffolds with tissue-specific stiffness, along with vasculature to rapidly recreate the TME with high accuracy and reproducibility.[12,32] Techniques such as extrusion and droplet-based bioprinting allow for the spatial patterning of multiple cell populations followed by photopolymerization to provide the tissue-mimetic mechanical stiffness and stability for the constructs.[33] PBs comprising photopolymerizable natural biomaterials combined with leachable thixotropic biomaterials can provide porous constructs with improved biocompatibility after photopolymerization for modeling the impact of the pore size on cell migration and ECM remodeling. Even though extrusion-based sacrificial bioprinting[34] can provide hollow channels for the development of vascularized models,[35] the need for a supporting bath and lack of printing resolution can be overcome by utilizing PBs with stereolithography. PB formulations can be tuned for optimal printability and cell viability depending on the 3D bioprinting technique utilized. Cancer tissue specificity can be achieved by recapitulating the tumor heterogeneity and microenvironment by incorporating tumor specific cells such as cancer cells, stromal cells, immune, vasculature, and ECM mimetic biochemical and physical cues.

Several reviews provide comprehensive overviews on photopolymerization chemistries,[24] PIs, photoabsorbers, printing parameters with PBs,[36] and photopolymerizable biomaterials utilized for various tissue engineering applications.[37,38] A few reviews are available in the literature on 3D bioprinting, which have highlighted the complexity of the TME[39,40] and ability of 3D bioprinting approaches[41−43] to recreate 3D tumor models. However, these articles offer minimal insight into PBs and have not adequately highlighted the utility of PBs in faithfully recapitulating the complexity of TME. The current article aims to provide an overview of popular bioprinting modalities for PBs and their reaction chemistries, bioink compositions specifically explored for TME recreation. The article begins with an introduction to TME complexity, followed by a comparison of the bioprinting approaches involving PBs relevant to tumor models, followed by the reported examples wherein PBs were successfully used to bioprint tumor models for cancer research involving drug screening and the study of cell−cell and cell−ECM interactions and metastasis.

2. TUMOR MICROENVIRONMENT COMPLEXITY

The TME, with its unique composition, architecture, and functionalities, supports the growth and invasion of cancer cells. The key components of the malignant TME include (a) ECM of the TME, (b) stromal cells of the TME, (c) tissue-

https://doi.org/10.1021/jacsau.3c00281
JACS Au 2023, 3, 2086−2106

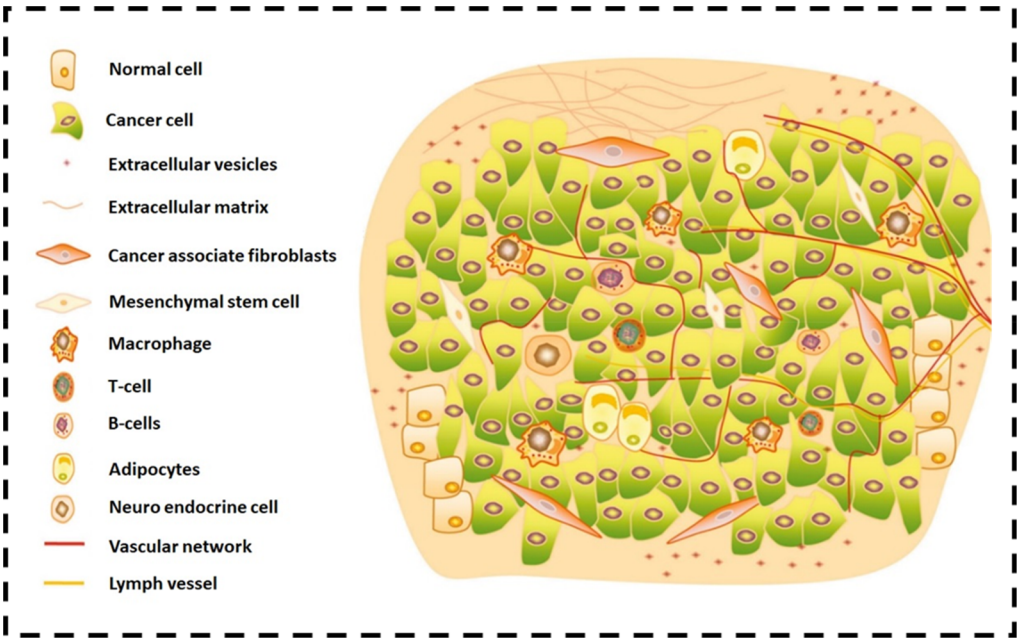

Figure 1. Components of the TME. The scheme represents multiple cellular and noncellular components present in the TME.[44] Reproduced with permission from ref 44 with license under CC BY 4.0 (https://creativecommons.org/licenses/by-nc/4.0/). No changes were made to the copyrighted material.

specific cancer cells, (d) biochemical and biophysical gradients, and (e) leaky vasculature[44] (Figure 1). ECM of the TME primarily comprises collagens, proteoglycans (proteins with glycosaminoglycans), and glycoproteins (proteins with oligosaccharides).[45] The tumor ECM is characterized by increased collagen type I expression and its increased fibrillar diameter.[46] The cross-linking by lysyl oxidase promotes collagen alignment, which in turn offers a path for tumor cell migration. In most carcinomas (epithelial origin cancers), increased stiffness of ECM is associated with tumor invasiveness.[47] Apart from collagen, several proteoglycans are upregulated in the TME, which provides the cancer cells with binding sites for the growth factors and cytokines to support the growth of cancer cells and induction of angiogenesis.[48] Stroma represents the surrounding tissue of the tumor, comprising fibroblasts and immune cells that are initially attracted to the tumor site. Subsequently, these cells are altered to tumor-promoting phenotypes by cytokines and signaling molecules secreted by cancer cells, which in turn helps in desmoplasia mediated by cancer-associated fibroblasts[49] (CAFs) and upregulated secretion of angiogenic factors by tumor-associated macrophages (TAMs).[50] Cancer cells also secrete exosomes with specific integrins, which initiate endocrine signaling to upregulate the endothelial permeability. This helps create a microenvironment that is suited for seeding metastatic cancer cells and allowing secondary tumor growth. The viscoelastic character of metastatic cancer cells and upregulated MMPs, and the overall matrisome, help in the progression of metastasis. Identification of matrisome patterns for several cancer types compared to their normal tissue types further enhances cancer prognosis and effective therapeutic strategies for metastatic cancers.[51] The use of biomaterials to recreate the 3D tissue models without the PBs are reviewed elsewhere.[52,53] In the following section, we discuss the commonly used bioprinting approaches using PBs for cancer modeling.

3. BIOPRINTING APPROACHES FOR PHOTOPOLYMERIZABLE BIOINKS

Bioprinting of *in vitro* 3D tumor models involves the usage of cell-laden bioinks, leading to limited availability of bioinks. The main bioink components are mostly limited to cytocompatible hydrogels to avoid cellular toxicity and provide a conducive matrix for cell functions. The working principles lead to three broad categories of printing procedures: extrusion, lithography (vat), and droplet (jetting) based bioprinting. In the following sections, we provide an overview of bioprinting approaches involving PBs and their wide range of applications and recent advances in PBs utility in bioprinting approaches (Figure 2).[36]

3.1. Extrusion-Based Bioprinting (EBB)

Extrusion-based bioprinting involving PBs has been widely explored for 3D bioprinted constructs for tissue engineering applications such as bone, cartilage, corneal, heart, liver,[54] vascular tubes, kidney, and vascular grafts.[21] EBB can be adapted with light-based photopolymerization of constructs after printing or during printing through a photopermeable nozzle for extrusion and deposition onto the substrate (Figure 2a–c). The bioink for extrusion bioprinting should be shear thinning and thixotropic, with low adhesion and surface tension for microextrusion. The bioink should exhibit rapid gelation kinetics and avoid droplet formation to maintain structural stability after the printing process.[55] The bioink typically uses thixotropic polymers for extrusion by means of pneumatic, piston-driven, or solenoid-based systems. Over the years, several researchers have optimized the printability of PBs for extrusion-based bioprinting. Bertassoni et al. optimized the extrusion-based bioprintability of GelMA (5–15 wt./v%) by precuring it for obtaining consistent fiber strands with high fidelity.[54] The usage of sacrificial bioink involving agarose,[56] PF127[57] printing along with PBs provided the ability to incorporate hollow channels, which can be utilized for developing endothelialized channels containing thick ECM mimetic constructs. Bhise et al. developed a spheroid-based

https://doi.org/10.1021/jacsau.3c00281
JACS Au 2023, 3, 2086–2106

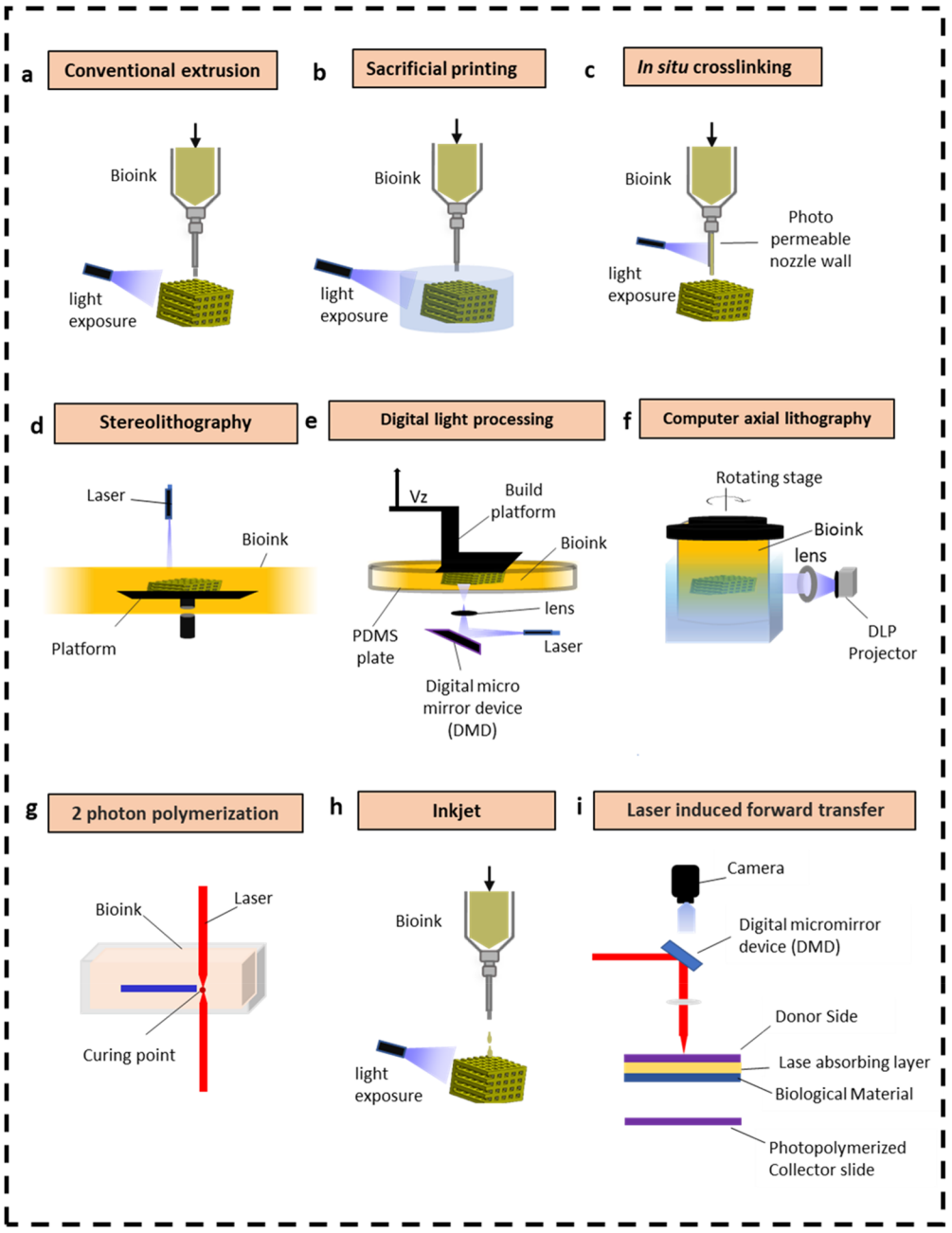

Figure 2. Schematic illustrating different types of bioprinting approaches involving PBs. (a) Conventional extrusion, (b) sacrificial, (C) extrusion with *in situ* cross-linking, (d) stereolithography (SLA), (e) digital light processing (DLP), (f) computer axial lithography (CAL), (g) 2 photon polymerization (2PP), (h) inkjet, and (i) laser-induced forward transfer (LIFT) techniques that use light to control the spatial organization of materials, cell-instructive factors, and cells toward the engineering of tissues. Reprinted with permission from ref 36. Copyright 2020 American Chemical Society.

bioprinted liver-on-chip device for acute toxicity screening.[58] These models can be adopted to engineer the primary tumor models of specific tissues to understand the progression of metastasis or as means to understand the impact of carcinogens to induce tumor-specific phenotypes apart from applications such as evaluation of the accumulated toxicity and therapeutic effects of several drug candidates. PBs can address several challenges and needs associated with 3D bioprinted constructs, such as mechanical properties and their tunability via photopolymerization induced covalent curing compared to other methods such as physical, ionic, and enzymatic curing strategies involved in non-PB-based inks. Usage of photocurable, thermoresponsive natural biomaterials such as GelMA-containing PBs can be tuned for extrusion vs vat-based printing. For example, at a given polymer concentration (10−15% is typically used), the PB can be used for extrusion-based 3D bioprinting by partially precuring or reducing the temperature of printing (<20 °C). In contrast, the PB can be used at 37 °C for vat-based 3D bioprinting. PBs involving extrusion-based bioprinting provide an ability to recapitulate tumor microenvironment by providing the ability to create biochemical and mechanical gradients via photoabsorber-induced cross-linking density gradient. Perfusable volumetric tumor models can be achieved via coaxial bioprinting followed

https://doi.org/10.1021/jacsau.3c00281
JACS Au 2023, 3, 2086−2106

by light-mediated curing and removal of the sacrificial ink post curing. Cell to ECM interactions can be recapitulated by using photocurable ECM mimetic natural polymers at varying concentrations. Cell to cell interactions can be recapitulated by spatially patterning the different cell types layer by layer or using a semipermeable membrane to separate 3D bioprinted constructs to recapitulate juxtracrine or paracrine interactions, respectively. Extrusion bioprinting of PBs combined with other printing modalities and microfluidics can recapitulate the physiological flow conditions and multicellular vascularized largescale tissues in a high throughput manner for efficient recapitulation of TME.

3.2. Lithography (Vat)-Based Bioprinting (LBB)

SLA, DLP, 2PP, and computer axial lithography (CAL) represent the widely used vat based photopolymerization strategies for cell-laden lithography-based printing (Figure 2d−g). SLA involves point-by-point laser scanning to cure non viscous PBs leading to increased printing time compared to DLP. DLP mainly involves layer-by-layer curing of bioink through digital micromirror device (DMD) generated masks, leading to rapid printing. Computed axial lithography (CAL) uses a DLP projector with a rotating stage to cure the PBs in 3D with rapid printing speed. 2PP involves the use of a two-photon infrared (IR) laser to cure the PBs. The precise curing at the focal plane provides a high resolution of up to 100 nm compared to other lithography-based techniques involving UV and visible light-based PIs. For optimal lithography-based printability, PBs should contain water-soluble PIs with minimal cytotoxicity and other additives, such as photoabsorbers, to avoid excess curing during layer-by-layer printing.[19] The PBs viscosity should be sufficient to maintain the homogeneous distribution of cells and the other bioink components to minimize heterogeneity in the 3D construct while printing.[59] Recently, to realize a high cellular density containing perfusable, vascularized tissue construct (1×10^7 cells/ml), a density gradient medium (iodixanol) was added to 5% GelMA to act as a refractive index modifier. Iodixanol reduced light scattering and improved the resolution of DLP bioprinting of high cell density construct.[60] Vat-based photopolymerization has been explored for applications such as skin, liver, bone, nerve, and cartilage tissue engineering due to the ability to create hierarchical structures, high-resolution cell patterning, and surface topography for complex 3D structures development, which can be leveraged to recreate the TME of several tumor varities.[61] Li et al. developed a support bath-based DLP system to print structures with soft ECM-like stiffness (4.3 kPa), which can minimize damage to large structures by compression or stretching.[62] Recently, Xolography-based printing enabled ten times higher resolution compared to CAL and provided four to five times faster volume generation compared 2PP.[63] Currently, volumetric bioprinting approaches are limited by their inability to print multiple materials, which was addressed by a recent development involving the photopolymerization of orderly extruded multimaterials (POEM) to create multimaterial cell-laden constructs. Even though the bioink utilized supported cell viability only up to 5 days, the approach can be extended to other cytocompatible bioinks for PBs multimaterial bioprinting.[64] Multimaterial-based lithography can provide an excellent opportunity to recreate the TME rapidly and recapitulate vascularized volumetric tumor models in a high throughput manner. Mechanical and biochemical gradients and microvasculature can be realized using advanced vat-based technologies[65] leading to a recapitulation of the TME and facilitating immune cell infiltration for investigating aspects of immuno-oncology and developing personalized medicine platforms. A combination of different bioprinting modalities and improved multimaterial-based lithography-based bioprinting can provide improved ways of recreating the multicellular TME in a high throughput manner and reproducibility.

PBs with photopolymerizable biomaterials can be modified with light responsive functional groups to spatiotemporally control the degradability of 3D bioprinted constructs to mimic the dynamic ECM remodeling of the TME compared to non-PBs. The conjugation of natural ECM mimetic peptides to PBs derived from synthetic biomaterials can afford MMP-dependent ECM remodeling of tumors to understand the key cellular signaling pathways and to develop 3D tumor models for monitoring the efficacy of MMP inhibitors.[35] Stereolithography-based PBs are the only bioinks which can provide improved lateral resolution up to 10 μm in the $X-Y$ plane and limited only by the pixel of the projector used for the curing. Improving the pixel resolution can provide a means to rapidly recapitulate the architectural features for understanding cancer cell migration and modulation of phenotype.

3.3. Droplet (Jetting)-Based Bioprinting (DBB)

DBB mainly involves low viscous bioink passed through a nozzle to create droplets.[12] Several droplet bioprinting modalities such as inkjet (Figure 2h), acoustic droplet, micro valve[66]-based bioprinters can be adapted for depositing precise volumes for spheroids 3D bioprinting for high throughput drug screening.[67] DBB offers precise volume control and better resolution (50 μm) compared to EBB but is associated with the lack of availability of a wide range of bioinks owing to the need for low viscosity (<10 mPa.s) for printability. Strategies such as laser-assisted bioprinting can provide means to create droplets for inks with up to 300 mPa.s viscosity but are limited by the cost. Laser-assisted bioprinting mainly involves a laser-induced forward transfer (LIFT) (Figure 2i) method involving a nozzle-free and contactless procedure for material jetting on to a substrate to generate droplets which can be cured using photopolymerization to realize the layer-by-layer fabrication of 3D constructs. Several studies have explored laser-assisted bioprinting for cancer studies.[16,68] Recently, to improve the printability and resolution of low viscous bioinks, usage of upward ejection-based bioprinting involving 5% GelMA provided better control over droplet spreading and improved resolution compared to downward bioprinting.[22] Chen et al. developed an acoustics-based drop-on-demand bioprinter to print high cell density (>10^8 cells/mL) multicellular patterning to realize better functional disease models.[69] Inkjet printing can also provide opportunities to isolate single cells for drug screening and gene expression analysis for intratumoral heterogeneity analysis. Lee et al. developed a nondestructive way for inkjet-based printing of 3−10 wt % GelMA using sonication to develop physiologically relevant constructs which can be adapted to several polymers for imparting the inkjet-based printability.[70] PBs involving droplet-based bioprinting can facilitate the ability to miniaturize tumor models and recapitulate multicellular and cell−ECM interactions. Due to prolonged printing times, large-scale constructs can be difficult to recapitulate but provide an excellent opportunity to create multicellular spheroids to understand the complex cellular interactions and high throughput drug screening. Droplet-

https://doi.org/10.1021/jacsau.3c00281
JACS Au 2023, 3, 2086−2106

based bioprinting involving PBs offers the ability to mimic cell−ECM, cell−cell interactions, but lacks in vascularized volumetric tumor models with perfusion. DBB can be combined with stereolithography to recapitulate tumor cell migration and invasion by depositing multicellular spheroids into preconstructed DLP based perfusable structures to understand the impact of various novel therapeutics and disease biology monitoring in high throughput formats. A comparison of PBs bioprinting modalities along with their ability to recreate TME is provided in Table 1.

4. PHOTOPOLYMERIZABLE BIOINK COMPONENTS

PBs comprise biomaterials with reactive groups, a PI, rheological modifiers such as gelatin, pluronic F127, Xanthum gum,[72] and methyl cellulose,[73] and refractive index modifiers such as iodixanol[74] and photoabsorber at varying concentrations depending on the printing approach used[36] (Figure 3 a). PI and photoabsorber play a critical role in modulating the construct stability, fidelity, resolution, and mechanical properties by controlling the cross-linking density through light attenuation.[27,75] PI provides the free radicals for polymerization involving different wavelengths for initiation. 2-Hydroxy-4′-(2-hydroxyethoxy)-2-methylpropiophenone (Irgacure2959), responsive to 365 nm, and lithium phenyl-2,4,6-trimethylbenzoylphosphinate (LAP), responsive to 405 nm, are the most widely adopted PI for *in vitro* 3D bioprinted tumor models. LAP provides improved cytocompatibility and reduced genotoxicity, as it requires visible light compared to Irgacure2959. Increased PI concentration can lead to rapid curing and lower penetration depth of the light due to scattering by polymerized layer.[61] LAP was shown to result in improved cell viability (80%) than Irgacure2959 (25%) at a concentration of 0.7 wt %.[76] Photoabsorbers avoid excess cross-linking by absorbing curing wavelength or reacting with free radicals generated. It prevents polymer curing induced via light scattering into the lateral, longitudinal plane of exposure to form highly convoluted structures in vat-based printing.[77] Photoabsorbers such as tartrazine,[59] Ponceau 4R29,[78] phenol red, and Orange G afford better printability of constructs with improved multichannel and vascular networks by avoiding excess curing, as demonstrated in several studies.[77,79] Even though it is not widely adopted for PBs for cancer research, the content of photoabsorber can be optimized for several reported PBs to recreate TMEs with increased complexity in 3D *in vitro* models involving vascularized microfluidic channels.

Biomaterial constituents primarily determine the biological and mechanical properties of the bioink, which determine cell viability, printability, ability to mimic the tumor *in vivo*, and long-term structural integrity.[80] Gelatin, hyaluronic acid, chitosan, alginate, and silk fibroin[81] comprise the widely used natural materials for PBs along with synthetic biomaterials such as poly(ethylene glycol) (PEG) and poly(vinyl acetate) (PVA). These biomaterials attain sensitivity to light-based cross-linking when chemically modified with reactive functional moieties such as methacrylate, norbornene, or glycidyl methacrylate, in combination with a specific wavelength and a corresponding PI for bioprinting[30] (Figure 3 b).

Gelatin methacryloyl (GelMA)[82] is the most widely used natural biomaterial for PBs used for cancer tissue bioprinting, followed by hyaluronic acid methacrylate (HAMA), as they are ECM-derived molecules that provide the cell-binding integrin sites and glycosaminoglycans, respectively. GelMA (5−10%)

Table 1. Comparison of 3D Bioprinting Modalities with PBs for TME Recapitulation[35,71]

Printing Strategy	Bioprinting Method	Bioink Properties	Light Exposure	Advantages	Limitations	TME Recapitulated
Extrusion	Conventional extrusion (pneumatic), *in situ* cross-linking based, sacrificial Bioprinting	Viscous bioinks (30 mPa *s* to 6×10^7 mPa.s), Rheological additives, Sacrificial materials, Thixotropic materials	Pre, post, and during printing	Multi material bioprinting, Spatial patterning, Affordability, Wide range of bioinks available	Limited resolution (>100 μm), Slow printing speed	Cell−ECM interactions, cell coculture, vasculature, and biochemical gradient
Lithography (Vat)	DLP, SLA, CAL, 2PP, xolography, POEM	Moderately viscous (<10^4 mPa.s) bioinks	Point to point (SLA), layer by layer (DLP), continuous (CAL)	High resolution, Surface topography with moderate printing conditions; high precision structures	Limited multimaterial printability, cytotoxic PI with high cost, lack of tissue-specific bioinks	Cell−ECM interactions, cell coculture, vasculature, and mechanical gradient
Droplet (Jetting)	Inkjet, micro valve based, laser-induced forward transfer	Non viscous bioinks (<10 mPa.s) and rheopectic behavior for inkjet bioprinting and up to 300 mPa.s for LIFT based droplet generation	Post printing	Precise volume control, Multiple cells spatial patterning	Low resolution, limited available bioinks, Difficulty in thick constructs printability	Cell−ECM interactions, cell coculture

https://doi.org/10.1021/jacsau.3c00281
JACS Au 2023, 3, 2086−2106

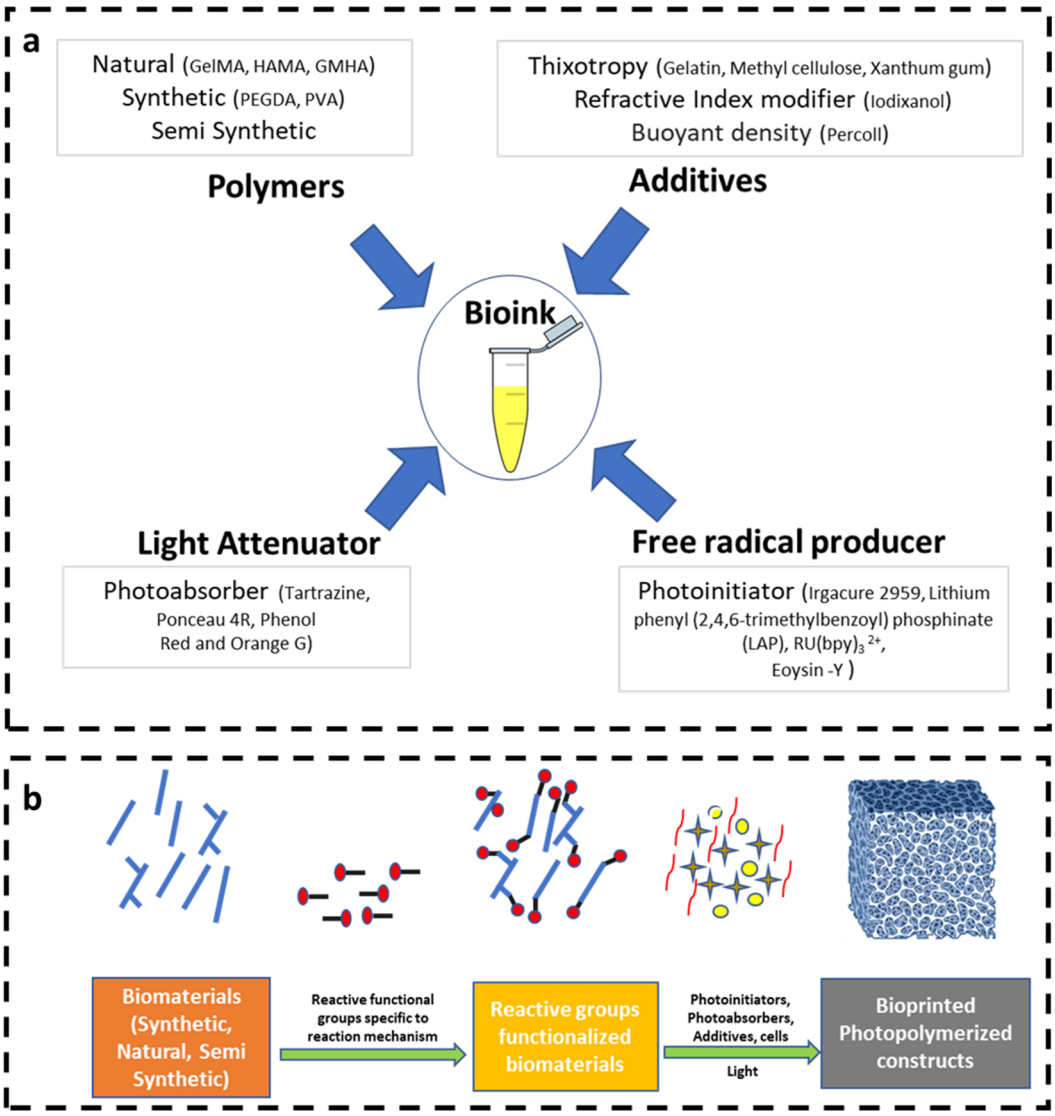

Figure 3. Photopolymerizable biomaterials synthesis and PBs components. (a) PBs bioink components comprising polymers, additives, light attenuators, and free radical producer.[30,78,79] (b) Workflow for PB development for 3D bioprinting.

alone or in combination with other synthetic and natural biomaterials provided the optimal printability, biochemical, and mechanical cues for various cancer bioprinted 3D models. Acrylated polyethylene glycol represents the widely used synthetic biomaterial in PBs for cancer *in vitro* models. The optimal biocompatibility, lot-to-lot consistency, high printing resolution, and mechanical tunability of synthetic polymers were explored to understand the effect of substrate stiffness,[83] topography,[84] and geometrical cues[85] on cancer cells. A lack of ECM components and a high degree of cross-linking can be toxic for synthetic polymers cell-laden bioprinting depending upon the polymer molecular weight and concentration utilized. The control over polymer concentration and degree of cross-linking of light-sensitive biomaterials provide an opportunity for the incorporation of chemical gradients with high cell densities and tissue-mimetic vasculature, rendering PB-based bioprinting highly promising.[10] On the contrary, the typical limitations of natural biomaterials include lot-to-lot variability and limited mechanical stability. These issues can be addressed by several approaches such as usage of ECM mimetic peptide conjugated synthetic polymers,[86] semisynthetic biomaterials, and multicomponent bioinks[87] as alternatives for better mechanical stability of 3D bioprinted constructs. Further, recent advances in recombinant DNA technology and polymer reaction chemistry led to more relevant biomaterials development, such as photopolymerizable recombinant collagen[88] (with monodispersity) and photopolymerizable decellularized ECM.[89] These biomaterials can provide more relevant ECM mimics for cancer research progress by using PB-based bioprinting. Another key concern in this field is using far UV light for photopolymerization and the resultant genetic and phenotypic changes. This limitation has motivated research to develop PIs that are responsive to visible[90−92] or near-infrared radiation[93,94] (NIR).

The PBs utilized for bioprinting are mainly polymerized via mechanisms such as free radical-based chain growth, Thiol−ene-based clickable step growth, and photo radical-based coupling. Free radicals-based polymerization is the most adapted form of cross-linking for fabricating tumor models. It involves the formation of a kinetic chain connecting the reactive groups of the polymers leading to a cross-linked structure.[36] Thiol−ene click reaction chemistry involves

https://doi.org/10.1021/jacsau.3c00281
JACS Au 2023, 3, 2086−2106

sulfhydryl groups and avoids oxygen-based inhibition of photopolymerization. It allows homogeneous network formation compared to chain growth-based cross-linking. Thiol−ene-based reactions have not been widely explored for tumor models. The utilization of acrylate-modified polymers along with sulfhydryl groups for photopolymerization can yield a mixed model of photopolymerization involving both chain and step-growth polymerization, which can help in tuning the mechanical properties and cross-linking network formation.[24] The photo radical coupling mechanism primarily involves the use of polymers containing phenol groups, which are further oxidized by photosensitizers to initiate the polymerization of reactive polymer groups. Optimization of bioink printability is essential due to the excess generation of reactive oxygen species and the large time requirement for curing, which can lead to reduced cell viability. Redox coupling-based curing mechanisms are not widely explored for cancer research and other tissue engineering applications. In terms of cell viability, free radical-based cross-linking can lead to higher cell death due to increased free radical generation and unreacted acrylate groups[95] compared to redox coupling and thiol−ene-based reaction chemistries. Table 2 provides a summary of the chemistries, reaction kinetics, and reactive groups for different reaction chemistries.

Overall, the bioink should provide good cell viability and minimally alter their genetic and phenotypic characteristics during and after the printing process.[66] The optimal bioink for 3D bioprinting for cancer tissue generation should comprise multiple components to support the structural stability of the *in vitro* 3D models while mimicking the TME. Table 3 compiles the widely utilized polymers and their advantages, disadvantages, and working concentration relevant to cancer tissue bioprinting. In the following sections, we summarize the PBs-based bioprinted models popularly utilized for cancer tissue engineering.

5. APPLICATIONS OF PHOTOPOLYMERIZABLE BIOINKS IN 3D BIOPRINTED TUMOR MODELS

A key focus of cancer research is understanding TME complexity to create advanced therapeutic approaches to avoid tumor recurrence. 3D models developed to investigate the TME have primarily focused on cell−cell interactions, cell−ECM interactions to elucidate mechanisms of metastasis, and advanced drug screening platforms to identify novel therapeutics. Some of the reported work in 3D cancer models have explored opportunities in precision medicine,[97,98] but there is little work on 3D bioprinted models. In this section, we summarize the latest developments in cancer drug screening models, metastasis studies, cell−cell interactions, and cell−ECM interactions studies (Scheme 1) involving PBs and the corresponding bioprinting modalities, as summarized in Table 4.

5.1. Drug-Screening Models

More than 95% of cancer drugs fail in clinical translation, despite favorable preclinical trials.[116,117] It is widely recognized that the current preclinical models lack the immunogenic, human tissue complexity,[118] underscoring the importance of developing 3D tumor models to bridge the preclinical to clinical translation gap of cancer drugs.[6,7] Several studies involving 3D models represented more relevant *in vivo* drug responses in the tumor models like 3D spheroids,[119] scaffold-based,[97] and cell-laden bioprinted constructs.[120] A combina-

Table 2. Reaction Chemistries and Polymer Backbones for PBs[21,36]

Reaction Type	Reaction Kinetics	Remarks	Polymer Backbone Functional Groups
Free radical photopolymerization	Faster compared to other reaction chemistries. Lacks reaction control and homogeneous network formation.	Free radical polymerization involves initiation, propagation, and termination, with each stage having different kinetics. High intensity of wavelength and excess free radicals can damage the cells leading to increased toxicity for cells. Oxygen-based inhibition reaction can be tackled by incorporating antioxidants in the bioink.	Methacrylate, acrylate, N-vinyl amide
Thiol−ene photopolymerization	Slower than the free radical method. Better control over network formation.	The degree of cross-linking is modulated by the concentration of cross-linker used rather than the concentration of reactive groups (Mostly step growth) Provides better control over spatial and temporal cross-linking. Not inhibited by the presence of oxygen. The long-term stability of the reagent can be lost due to disulfide group oxidation.	Norbornene, vinyl ether, propenyl ether, alkene, vinyl ester, N-vinyl amide, allyl ether, acrylate, maleimide, methacrylate
Redox Cross-linking	Slower than the thiol−ene reaction. Better control over network formation.	Polymers modified with phenol groups can be photocross-linked in the presence of a photosensitizer via photooxidation and subsequent radical coupling between reactive groups	Tyrosine, tyramine

https://doi.org/10.1021/jacsau.3c00281
JACS Au 2023, 3, 2086−2106

Table 3. Classification of Light-Based Biomaterials for Cancer Tissue Bioprinting[96]

Biomaterial type	Light-Based Biomaterials	Advantages	Disadvantages
Natural	Gelatin methacryloyl (Most abundant) (5−15 wt.%), Hyaluronic acid methacrylate (0.25−2.5 wt.%)	ECM biochemical and mechanical cues mimic	Lot to lot variability, lack of *in vivo* specific ECM densities utilization
Synthetic	Polyethylene glycol diacrylates (20 wt.%) (Most abundant), Polyvinyl methacrylate	Mechanical stability, stiffness gradient properties tunability	Lack of ECM mimic
Semisynthetic	Synthetic polymers modified with cell binding sites	Controllable mechanical properties, tunability compared to natural materials	Lack of ECM recapitulation with respect to architecture and concentration
Multicomponent	Combination of the above natural, synthetic, and semisynthetic materials	ECM mimic and mechanical stability. Better tunability for printing	Not a perfect ECM mimic for cells. Rheological additives utilization can elicit an unintended response.

Scheme 1. Schematic Representation of the Tumor Microenvironment Recapitulation Capabilities of 3D Bioprinted *In Vitro* Models Involving Photopolymerizable Bioinks

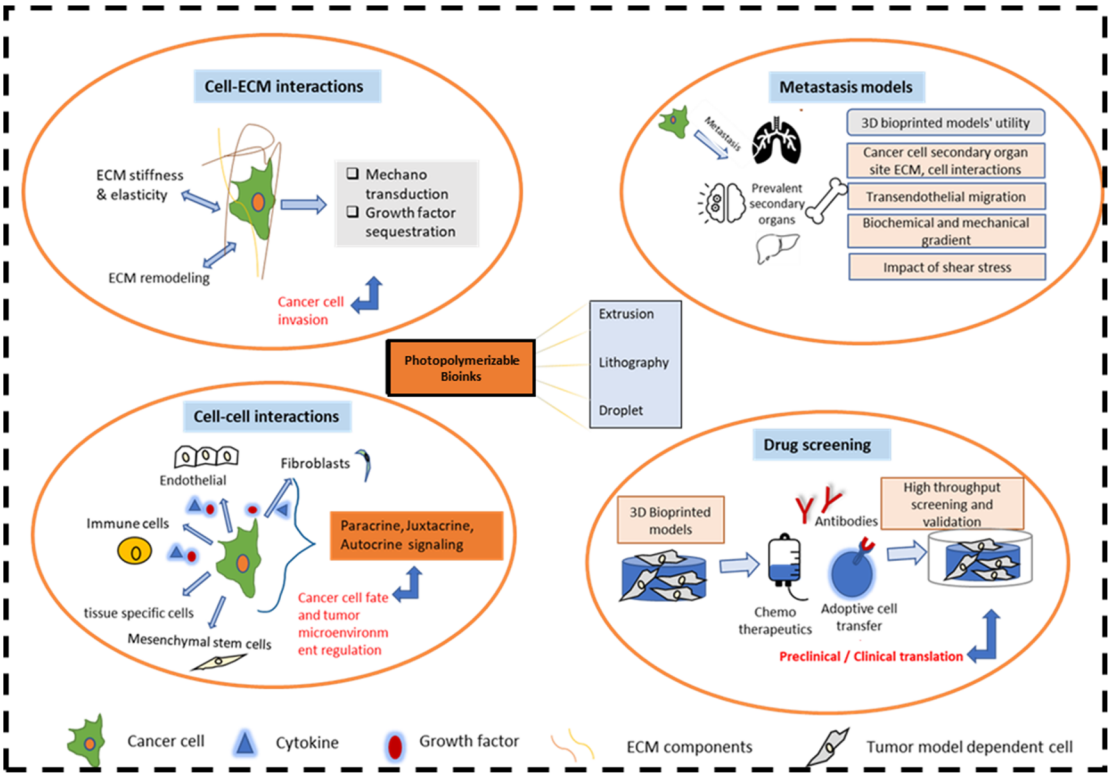

tion of photopolymerization-based bioprinting along with other bioprinting approaches such as laser-based, extrusion-based, inkjet bioprinting, and microfluidics can provide better resolution, size control, and reproducibility for 3D models for the rapid screening of drugs. Combining sacrificial extrusion bioprinting with photopolymerization, Zhang's group created a model for ductal carcinoma *in situ* using MCF7 cells[34] seeded on a hollow ECM mimicking channel. In another study, a lymphangiogenic model was developed by incorporating metastatic MDA-MB-231 breast cancer cells into GelMA, forming a hollow channel. Lymphatic microvascular endothelial cells (LECs) were seeded in to the channel to establish a lymphangiogenesis model.[56] The above model can be explored to develop novel antilymphangiogenesis followed by high throughput evaluation of the efficacy. In another study using coaxial bioprinting, a blood and lymphatic vessel pair was developed to understand the diffusion kinetics of drug molecules in TME under perfusion. PEG diacrylate (PEGDA) and 8-arm polyethylene glycol-octaacrylate (PEGOA), along with 5−7% GelMA and 3 wt % alginate, were used as bioink components for fabricating blood and lymphatic vessels, respectively. A multilayer, concentric, coaxial nozzle was used for codelivery of the bioink with $CaCl_2$ solution as the cross-linking agent leading to immediately cross-link the extruded hollow channels, which were embedded in MCF7 cell-laden GelMA solution followed by curing to establish a tumor on a chip. Furthermore, the incorporation of the lymphatic channel improved MCF-7 cell viability compared to the blood vessel alone, demonstrating the importance of recapitulating the rapid removal of doxorubicin through lymphatics.[109] These models can be explored to mimic the mass transport mechanisms of different macromolecules and chemotherapeutics. By incorporating TME-specific ECM components and flow conditions, these models can help identify new potential therapeutic approaches for ductal carcinoma *in situ* (DCIS), which focus on antiangiogenic and lymphangiogenesis strategies to reduce metastatic breast cancer progression. Heinrich et al. fabricated a 3D model for the study of glioblastoma-macrophage interactions by incorporating glioblastoma cells surrounded by mouse macrophages

https://doi.org/10.1021/jacsau.3c00281
JACS Au 2023, 3, 2086−2106

Table 4. 3D Bioprinted Tumor Models Prepared with PBs Used for Cancer Modeling

Cancer Addressed	Bioink Components/ Composition	Cell Type/Origin	Bioprinting Approach	Model Application				Remarks	Ref
				Cell−Cell Interactions	Cell−ECM Interactions	Metastasis	Drug Screening		
Brain	3% GelMA and 4% gelatin	Raw 264.7, GL261 glioblastoma cells	Extrusion bioprinting	X			X	3D model with upregulated expression of glioblastoma multiforme (GBM) specific genes was established when glioblastoma cells were cocultured with macrophages to study the role of immune-cancer cell interactions in GBM progression.	99
	5, 10% GelMA, 0.5, 1% GMHA	Human patient-derived glioblastoma stem cells (TS576), CW468, HUVEC	DLP (Digital light processing)	X	X		X	3D model to understand the role of ECM stiffness on individual glioblastoma and HUVEC coculture for different subtypes of GBM recapitulation *in vitro*.	60
	4% GelMA and 0.5% GMHA	Astrocytes, NSC, Glioblastoma stem cells, Macrophages	DLP	X			X	3D bioprinted glioblastoma model with *in vivo* relevant transcriptional profiles compared to multicellular spheroid cultures.	100
Breast	5% GelMA, 8% Agarose	MCF7	Sacrificial extrusion-based bioprinting		X		X	Breast ductal carcinoma in situ (DICS) model was developed by combining photopolymerization with sacrificial bioprinting to recreate the complexity of DICS and its early stage ECM changes identification.	34
	5% GelMA, 8% Agarose	MDA-MB-231, Lymphatic endothelial cells (LECs)	Sacrificial extrusion-based bioprinting	X	X		X	MDA-MB-231 cells were embedded in ECM-like GelMA surrounding the LECs seeded channel to recapitulate the cell−cell interactions and behavior of individual cell types under the influence of VEGF C.	56
	35% PEGDA700, 7% GelMA	MCF7, HUVEC	Multimaterial DLP	X	X		X	A DLP-based microfluidics-enabled multimaterial rapid bioprinting of 3D models was achieved, which can be useful for recreating multicellular interactions, biophysical and chemical gradients for TME studies	101
	10% GelMA ± 10% nHA, 15% GelMA ± 10% nHA	MDA-MB-231, MSCs, Osteoblasts	Stereolithography (SLA)	X		X		Bone matrices mimicking SLA-based osteoblasts or hMSC-laden 3D models supported breast cancer cell growth, reduced ALP activity, and increased VEGF secretion during the coculture of breast cancer cells compared to monocultures by recapitulating bone postmetastatic progression of breast cancer.	102
	5, 10, 15% GelMA ± 10% PEGDA700 or 5,10,15% nHA	MDAMB-231, HUVEC, MCF7, Osteoblasts	Laser direct writing (SLA)	X		X		A triculture vascularized SLA-based 3D scaffold model of breast cancer, endothelial, and osteoblast cells was developed to mimic transendothelial migration and cancer cell colonization in the metastatic site.	103
	5% GelMA, 5% GelMA and 1% Alginate	MDA-MB-231, HUVEC	Coaxial bioprinting	X				A tunable spheroid of MDA-MB-231 cells embedded with 180 μm fiber of HUVECs to develop a coculture system with high viability was established, which can be further helpful in complex 3D tumor models establishment for breast cancer research.	104
	5% GelMA, 5% Gelatin	Human breast cell line (MDA-MB-231), mouse osteoblast cell line (MC3T3-E1) (mouse cells), HUVEC	Coaxial extrusion bioprinting	X				A coaxial 3D bioprinted vascular channels with self-seeded endothelial cells were used to recreate the vasculature of the TME in 3D with angiogenesis toward cancer cells observed by day 15.	105
	3% Gelatin, 20% PEGDMA 1 kDa	MCF7	Droplet-based bioprinting	X			X	A 3D spheroid array model was developed using gelatin's thermoresponsive behavior. Concave wells were fabricated by depositing PEGDMA solution on thermally gelled cell-laden gelatin droplets, followed by inverting the PEGDMA concave well and liquefication by incubation at 37 °C for uniform cell spheroids formation.	106
	30% PEGDA700, PEG400 (20%), EtOH (49.5%)	MCF7	DLP with a microfluidic system	X			X	An array of multicellular tumor spheroids (MCTS) with varying ratios of multiple cell types were printed for anticancer drug evaluation.	107
	19% PEGDA 700 Da, 1% acrylic acid; 95% PEGDA 700 Da, 5% acrylic acid	Normal mammary epithelial cells (HMLE) or HMLE-Twist cells	DLP			X		A stiffness tunable scaffold was printed by using varying PEGDA concentrations for studying mammary epithelial cells and TWIST oncogene transformed cells migration ability in 2D vs 3D scaffolds. The 3D model relevance can be further increased by using growth factors and integrin sites incorporation in the PEGDA.	83
	8% GelMA	MCF7, Normal human dermal fibroblasts (NHDFs)	Dot Extrusion	X	X		X	Dot extrusion based paracrine and juxtacrine model for breast cancer cells and fibroblasts interaction and drug screening. This model can be adapted to several other cancers for disease models development	108

https://doi.org/10.1021/jacsau.3c00281
JACS Au 2023, 3, 2086−2106

Table 4. continued

Cancer Addressed	Bioink Components/ Composition	Cell Type/Origin	Bioprinting Approach	Model Application				Remarks	Ref
				Cell–Cell Interactions	Cell–ECM Interactions	Metastasis	Drug Screening		
	5 or 7% GelMA, 3% Alginate, 4% PEGOA or PEGDA	MCF7, HUVEC, HLEC	Coaxial bioprinting	X	X		X	A perfusable blood and lymphatic vessel pair surrounding the tumor cells 3D *in vitro* model was developed to recapitulate microcirculation to mimic the transport kinetics of drugs and biomolecules	109
	1–3% Porcine Breast tissue ECM (TDM), 0.5 wt % Alginate, 2.5–4 wt % GelMA, 0.15% Collagen 1	MCF7, adipose derived mesenchymal stem cells (hAMSCs)	Extrusion bioprinting	X	X		X	Extrusion-based 3D bioprinted breast tumor model containing porcine breast derived ECM along with GelMA, alginate and collagen I for improved printability and biomimicry.	110
Cervical	20% PEGDA 700, 1% LAP, 0.01% TEMPO, 0.1% HBSC solution	Murine 10 T1/2, Hela cells	SLA			X		A 3D model for probing the impact of geometrical cues on cancer cell migration and morphology during metastasis was developed	84
Liver	5% GelMA and 2.5% GelMA and 1% Glycidyl methacrylate hyaluronic acid (GMHA)	HepG2, 10 T1/2 (mouse fibroblasts), HUVEC	Microscale Continuous Optical Bioprinting (DLP)	X			X	A vascularized 3D liver tissue model was developed with anastomosis for drug screening and vascularized organ development. The model can be extended to other tissues for disease modeling.	111
	6% GelMA	Human Hepatocellular Carcinoma cell line C3A	Acoustics based Levitation method	X			X	Acoustics-based levitation of cells utilized to create 3D cellular clusters followed by GelMA-based curing to obtain spheroids for high throughput drug screening	112
Lung cancer	5% GelMA, 1% fibrin, PLGA, AUNR (gold nanorods)	HUVEC, A549	Extrusion bioprinting	X	X	X	X	Vascularized 3D bioprinted lung cancer tumor model with spatiotemporal gradients of EGF recapitulated several aspects of TME, such as circulating tumor cell (CTC) intravasation, direct cancer cell migration, and proliferation.	113
	GelMA	A549	DLP bioprinting	X	X	X	X	A perfusable 3D tumor model was developed for lung cancer drug screening.	114
Oral	5% GelMA	Oral squamous epithelial cells, CAL 27, CAFs (patient-derived)	Acoustic droplet-based bioprinting	X				Acoustic droplet-based bioprinting postprinting photocuring was used to create a heterogeneous 3D model for cancer and stromal cell (CAFs) interactions and invasiveness study. Incorporating multiple cell types can further improve the model complexity.	69
Pancreas	5% GelMA	AR42J-B-13 acinar and ductal cells	Laser-induced forward transfer (LIFT)	X				A spheroid array-based 3D model to study the evolution of PDAC over time was developed, which can help screen the effect of biochemical and mechanical cues on PDAC development and cancer progression.	68
	8% GelMA	Human pancreatic cancer cell line (BxPC-3) and normal human dermal fibroblast cells (NHDFs)	Dot Extrusion	X	X		X	A high throughput multicellular spheroid model developed using ECM mimetic bioink to recapitulate the multicellular interactions for drug screening	115

https://doi.org/10.1021/jacsau.3c00281
JACS Au 2023, 3, 2086–2106

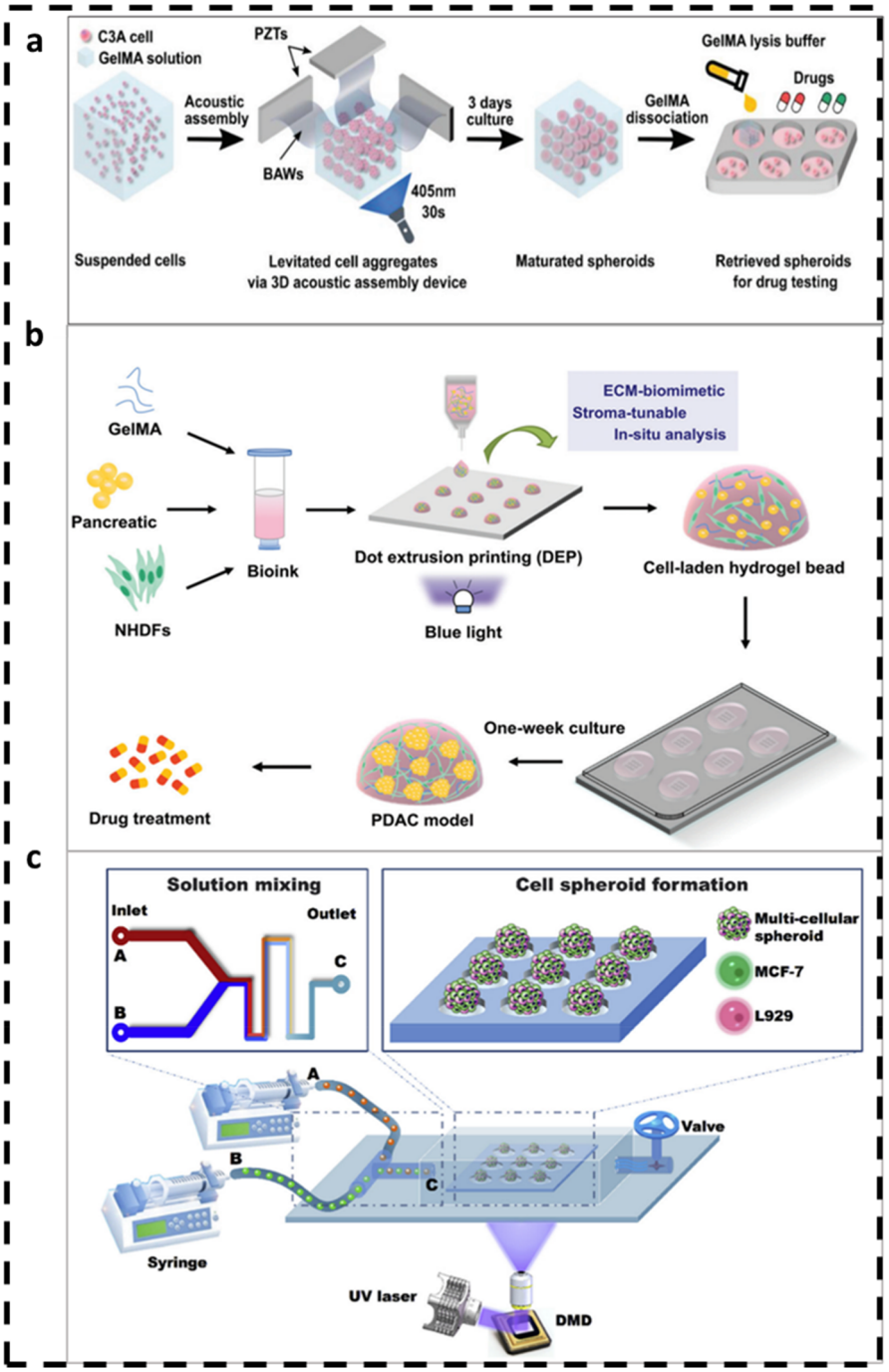

Figure 4. High throughput spheroids fabrication using photopolymerizable bioinks for drug screening. (a) GelMA based C3A cell spheroid formation using a 3D acoustic assembly device followed by photopolymerization for cell aggregate stabilization and retrieval of spheroids after 3 days for drug testing. Reproduced with permission from ref 112 with license under CC BY 4.0 (https://creativecommons.org/licenses/by-nc/4.0/). No changes were made to the copyrighted material. (b) Dot extrusion printing of pancreatic cancer BxPC-3 cells and normal human dermal fibroblast cells laden-GelMA hydrogel beads were grown for 1 week to form uniform-sized PDAC spheroid models for drug testing. Reproduced with permission from ref 115 with license under CC BY 4.0 (https://creativecommons.org/licenses/by-nc/4.0/). (c) A microfluid system integrated with DMD based microwell fabrication for generation of heterospheroid for high throughput drug screening using MCF7, L929 cells. Reprinted with permission from 107. Copyright 2019 Elsevier.

using extrusion-based bioprinting postphotocuring. This 3D model was used to evaluate the effect of the chemotherapeutic drug, carmustine (BCNU), and immunomodulatory drugs, such as colony-stimulating factor 1 (CSF1) and signal transducer and activator of transcription 6 (STAT6) inhibitors, on tumor and immune cells. The IC50 values under 3D conditions were found to be higher than those under 2D conditions for all drugs studied. Transcriptional mapping of the individual cells in 3D model revealed *in vivo* tumor-specific gene expression profiles.[99] In another study, Tang et al. developed a DLP-based 3D glioblastoma model by bioprinting glioblastoma stem cells (GSCs) with (tetra) or without (tri) human macrophages, surrounded with stromal cells, such as astrocytes and neuronal stem cells (NSCs). These 3D models

https://doi.org/10.1021/jacsau.3c00281
JACS Au 2023, 3, 2086−2106

and glioblastoma cell spheroid cultures were treated with epidermal growth factor receptor (EGFR) inhibitors such as erlotinib, gefitinib, and alkylating agent Temozolomide. Higher drug resistance was observed in the tetra-culture model compared to other conditions. The tetra-culture model expressed more tumor-relevant gene expression profiles seen *in vivo*, which can advance novel drug screening platforms targeting different aspects of TME interactions present in glioblastomas.[100] The same group also created a glioblastoma multiforme (GBM) model by incorporating human umbilical vein endothelial cells (HUVECs) and CW468 GSCs in GelMA and HAMA hydrogels of tumor-mimetic stiffness. They found that stiffer ECM (21 kPa) and the presence of HUVECs surrounding the glioblastoma cells prompted the resistance to Temozolomide.[60] In another study, using DLP-based 3D bioprinting, Chen's group recreated the microvasculature model of the liver, incorporating the liver cancer cell line HepG2, mouse fibroblasts, and HUVECs. The 3D bioprinted model was successfully anastomosed with host vasculature using the prevascularization induced by HUVECs. Further, such a 3D model can be useful for developing truly tumor-mimetic personalized drug screening platforms incorporating primary tissue cells and functional organ regeneration.[111] High throughput formation of spheroid can improve the rapid testing of drugs. Recently high throughput spheroid formation via acoustic assembly based device to form cellular aggregates in GelMA based bioink was explored for hepatocellular carcinoma spheroid formation and their retrieval for rapid drug screening (Figure 4a).[112] In another study, dot extrusion of pancreatic adeno carcinoma cells (PDAC) mixed with normal human dermal fibroblasts (NHDFs) was explored for heterospheroid formation in GelMA-based bioink for cell−ECM, cell−cell interactions, and drug screening (Figure 4b). Recently, Yang et al. created a multicellular tumor spheroid model by combining microfluidics and a DMD device with controllable cell ratios and spheroid sizes for anticancer drug screening. This model mimicked increased drug resistance in multicellular tumor spheroids (MCTSs) compared to individual cell spheroids of MCF7 and L929 cells (Figure 4c).[107] Matrigel-based spheroids are well explored for clinical drug screening, but these models lack in human relevant biochemical and mechanical cues provided by the ECM *in vivo*.[121] High throughput spheroid formation approaches involving photopolymerizable decellularized ECM-based bioinks can provide an advanced means to maintain tumor heterogeneity for patient-derived organoid drug screening. Advanced models containing bioprinted cancer on chips with dynamic flow and real time monitoring via biosensors can reduce the time for drug screening and enable patient-specific/personalized therapeutics. Together, the above studies demonstrate that the resolution and reproducibility of light-assisted bioprinting and emerging techniques such as multi-material-based lithographic bioprinting, combined with other bioprinting techniques and microfluidic approaches, can advance the field of cancer drug screening.

5.2. Metastasis Models

More than 90% of cancer-related deaths are attributed to tumor metastasis to the secondary sites.[117] Metastasis primarily involves key steps, such as (1) migration and invasion from the primary tumor site to the surrounding ECM matrix; (2) intravasation into the surrounding vasculature; (3) circulation via the bloodstream; (4) extravasation to the secondary site from vasculature; (5) colonization at secondary site and growth.[122] Each cancer is associated with a preference for metastasizing to specific organs depending upon the tumor's origin site and the cancer cell's genetic predisposition. Several genetic, epigenetic, chemical, physical, and phenotypic changes, such as epithelial to mesenchymal transition and cluster migration of tumor cells along with immune and stromal cells, can contribute to the migration of cancer cells to secondary organs.[123] Bone is a prevalent site for the migration of different types of cancer cells including breast, melanoma, lung, and prostate.[124] Zhang group created an SLA-based 3D printed model from GelMA and nanocrystalline hydroxyapatite (nHA) to mimic the bone matrix to study the postmetastatic interactions of MDA-MB-231 breast cancer cells with osteoblasts and bone marrow mesenchymal stem cells (MSCs). They observed upregulated secretion of vascular endothelial growth factors (VEGFs) during the coculture, which can augment angiogenesis and invasiveness of breast cancer cells.[102] The study explores the utility of an *in vitro* artificial bone mimetic model to understand colonization and growth of cancer cells. The model's complexity can be further increased by incorporating stromal cells and vasculature to understand the impact of cancer cells on other surrounding stromal tissues. In another study, the same group created a 3D vascularized model to study the transendothelial migration of highly invasive (MDA-MB-231) and noninvasive (MCF-7) breast cancer cells toward a bone matrix to understand the influence of endothelial cells on bone metastasis and invasion of breast cancer cells.[103] Meng et al. developed a tumor model by combining the individual 3D bioprinted modules to realize spatiotemporal biochemical gradients in a vascularized tumor model. The tumor model comprised an endothelialized microfluidic channel separating a linear array of 3D printed GelMA-based microcapsules of epidermal growth factor (EGFs) and VEGFs embedded in an ECM mimetic fibrin hydrogel. Stromal cells such as fibroblasts and A549 lung cancer cell clusters were included toward the EGFs capsule containing fibrin gel near the endothelialized microfluidic channel, and another side of the vascular channel was loaded with VEGFs capsules. The NIR-responsive GelMA-based microcapsules were used for controlled growth factor release to establish a biochemical gradient. They found that EGFs spatiotemporal release promoted cancer cell directed migration toward the gradient along with proliferation. VEGFs gradient promoted angiogenic sprouting from endothelialized channels. The introduction of flow allowed for the enrichment of circulating tumor cells. The model was able to recapitulate several aspects of cancer metastasis such as intravasation, invasion, and angiogenesis. The model can be adapted for other cancers by incorporating cancer tissue-specific ECM and tailoring the mechanical properties with PBs for enhancing the stability of the tissue constructs.[113] Notably, most of the 3D bioprinted models described above do not incorporate the impact of fluid flow-induced shear stress, a key physiological event *in vivo* influencing several cellular phenomena.[125] In contrast, there is vast scientific literature on biomicrofluidics-based research, wherein cells on or embedded within a thin layer of ECM are subjected to varying flow conditions. These devices enable the study of metastasis in several cancers.[126] However, these platforms are limited by their ability to recapitulate the complexity of the TME,[12] especially the spatial organization of cells and ECM characteristics such as differences in composition and stiffness,[127] anatomic scale,

https://doi.org/10.1021/jacsau.3c00281
JACS Au 2023, 3, 2086−2106

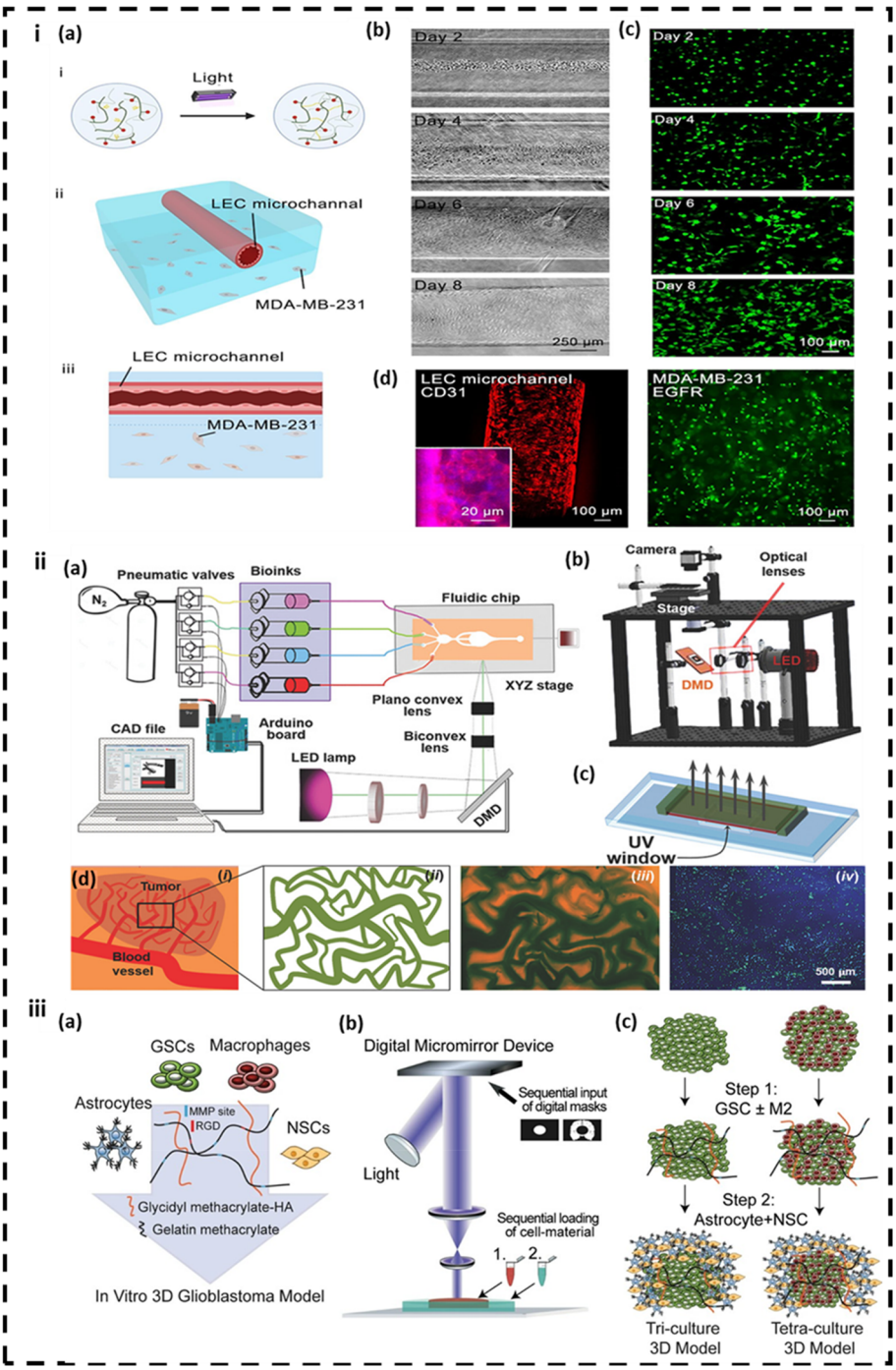

Figure 5. Examples of photopolymerization-based 3D bioprinted tumor models for different cancer types. (i) Breast cancer lymphangiogenesis model: (a) schematic for the 3D model; (b, c) bright field, fluorescence (live dead) images at different day points for MDA-MB-231 and LECs; (d) immunofluorescence imaging for CD31(red) and EGFR (green) markers for LECs and MDA-MB-231, respectively.[56] Reproduced with permission from Elsevier, Copyright 2021. (ii) (a) Multimaterial mask less stereolithographic bioprinter setup for the bioprinter along with microfluidic device. (b) Optical platform setup overview. (c) Schematic representing open-chamber microfluidic device for single-material printouts. (d) Schematic for the (i) tumor angiogenesis model, (ii) the mask for printing, (iii) PEGDA based bioprinted microvasculature; (iv) bioprinted GelMA microvascular bed with MCF7 cells (blue) and HUVECs (green) in channels. Reprinted with permission from ref 101. Copyright 2018 Wiley-VCH with license under CC BY 4.0 (https://creativecommons.org/licenses/by-nc/4.0/). No changes were made to the copyrighted material. (iii) Glioblastoma tumor model: (a) schematic for 3D glioblastoma model containing GSCs, macrophages, astrocytes, and neural stem cells (NSCs); (b) representation of digital micromirror device (DMD) chip-based bioprinting system used to produce the 3D glioblastoma model. Reproduced with permission from ref 133 with license under CC BY 4.0 (https://creativecommons.org/licenses/by-nc/4.0/). No changes were made to the copyrighted material.

and tunable cell−ECM interactions. With recent developments in light-based 3D bioprinting techniques such as DLP, these routes are emerging as promising approaches. These approaches can yield scaffolds of complex architecture with intricate features owing to their high printing resolution, vascular channels, and tissue-specific stiffness. The optically

https://doi.org/10.1021/jacsau.3c00281
JACS Au 2023, 3, 2086−2106

transparent bioinks utility in printing can be helpful in microscopic evaluation to assess the impact of physiological flow on metastasis and precision medicine.[59]

5.3. Cell−Cell Interaction Models

More than half of the TME is composed of stromal cells, which contribute to tumor progression or repression depending on the cell type and their interactions. It is now well recognized that understanding the cell-to-cell communications, including those involving stromal cells, in the TME can yield effective strategies to treat therapy-resistant cancers.[128] Cancer metastasis involves cell migration through the lymphatics and blood vessels to reach secondary organs. Understanding the interaction between endothelial and cancer cells can provide better strategies for treating metastatic cancers. To understand these interactions, the Zhang group prepared a 3D model by light-based sacrificial bioprinting to study the interactions between LECs and triple-negative breast cancer cells. As the lymphatic system serves as a major route for cancer metastasis, in the current model, sprouting and migration of LECs and MDA-MB-231 cells toward each other induced by VEGF- C was recapitulated in their model (Figure 5i).[56] In a different study, Xie et al. utilized coaxial bioprinting to prepare a coculture 3D model wherein HUVEC-laden microfibers were embedded in a mini-spheroid of MDA-MB-231 cells to study the interactions of endothelial and cancer cells. The actin filaments in HUVECs were elongated toward the cancer cells by day 13 in the coculture model compared to the monoculture of HUVECs in the 3D model.[104] Miri et al. developed a DLP-based multimaterial bioprinting approach using microfluidics. During this study, MCF-7 cells embedded in GelMA were patterned into a microvascular model, followed by the seeding of HUVECs to mimic the tumor angiogenesis model[101] (Figure 5ii). The model can be further improved in complexity by incorporating other cell types and biochemical and physical cues relevant to different cancer types. Recently, by using Carbopol as a support bath, a 3D tumor model involving neuroblastoma spheroids inside an endothelized GelMA-based channel was developed and monitored under dynamic and static culture conditions. This work aimed to establish a high throughput model to understand the molecular mechanisms of tumor proliferation, aggressiveness and drug response in neurblastoma.[129]

Immune cells and other stromal cells play crucial roles in TME regulation.[130] Understanding the mechanisms of cancer cell evasion from immune cell surveillance and their ability to modulate immune cell functions can provide novel approaches to target the TME. Henrich et al. prepared a mini-brain tumor model by encapsulating GL261 glioblastoma cells and glioblastoma-associated macrophages (GAMs) in 3D bioprinted GelMA hydrogels. The cell interactions were studied in the 3D model to elucidate the significance of paracrine and juxtracrine signaling. The model could successfully recapitulate the characteristic gene upregulation observed *in vivo* in both cell types with macrophage migration into the 3D printed glioblastoma mini brain within 24 h, along with increased cell proliferation.[99] As discussed above, in the context of drug screening models, Tang et al. developed a multicellular glioblastoma 3D model along with macrophages. They found that 3D bioprinted models better represented GBM-specific gene transcriptional profiles than did spheroid cultures for glioblastoma stem cells. Further, when macrophages were incorporated along with glioblastoma stem cells surrounded by NSCs and astrocytes (tetra-culture), the invasiveness of the glioblastoma cells was more compared to 3D models lacking macrophages (Figure 5iii).[60] In another study, laser-assisted bioprinting of pancreatic ductal carcinoma (PDAC) spheroids sandwiched between 5% GelMA was used to create a PDAC initiation model. This model mimicked the clinical scenario of acinar to ductal conversion with high reproducibility and larger controllable spheroid cell densities (10^8 cells/mL).[68] Currently, genetically engineered preclinical models have varied biology and altered immune interactions compared to humans. Immunocompromised mouse models are not useful for evaluating novel therapeutics such as adoptive cell transfer therapies (immunotherapy) for patient-derived xenograft.[118]

Moreover, individual cell−cell interactions are difficult to recapitulate in a preclinical mouse model. In contrast, 3D bioprinting techniques provide better alternatives to understanding and designing novel therapeutics and probing the effect of specific cell types on the TME. Current coculture models are majorly focused on static culture conditions, which do not reflect the pathophysiological conditions. Most of the current models for cell−cell interactions do not recapitulate the multicellular proportions and their heterogeneity in a dynamic flow condition, such as long-term immune and cancer cell crosstalk, circulating tumor cell interactions under physiologically relevant flow, and cellular heterogeneity. Developing tissue specific photocurable ECM can improve the understanding of cancer and secondary site cellular interactions with more *in vivo* relevance. Developing physiological flow-based conditions along with tumor environment-specific gradients can further advance the field of cancer research.

5.4. Cell−ECM Interaction Models

The biomolecular composition of the ECM plays a crucial role in defining the TME by influencing the stiffness and generating intratumor biophysical and chemical gradients. ECM composition also affects cellular motility through specific cell-matrix interactions. These events can profoundly influence cancer cell invasiveness and therapeutic efficacy of chemotherapeutic and radiation therapies for cancer treatment.[131] Understanding the role of the ECM and its remodeling by the tumor constituents can provide better therapeutic approaches for cancer research. The ECM in the TME is remodeled by several oxidases and proteinases depending on the cancer tissue origin and stage of cancer.[132] The Zhang group used GelMA to develop a 3D mammary ductlike hollow channel model to understand the ECM remodeling and influence of the MCF7 (luminal A type) breast cancer cells on mammary ductlike hollow structures. By day 14, the seeded MCF7 cells expressed collagen type IV without laminins, which is a key ECM molecule upregulated in late ductal carcinoma *in situ* (DCIS) and early invasive ductal carcinoma (IDC) during breast cancer progression and metastasis. By incorporating other ECM molecules in the model, it can be further improved for drug development, as discussed above for drug screening platforms.[34] Tang et al. developed DLP-based patient-specific glioblastoma tumor models by varying the compositions of GelMA and Glycidyl methacrylate hyaluronic acid (GMHA) fractions to mimic the different ECM stiffness. In this model, tumor cells were embedded in a matrix of stiffness similar to a GBM tumor (7 kPa) surrounded by an acellular ECM of either 2 (soft) or 21 kPa stiffness, which was further surrounded by either HUVECs or no cells. During the study, increased diffusive migration of

https://doi.org/10.1021/jacsau.3c00281
JACS Au 2023, 3, 2086−2106

cancer cells was promoted in the stiffer ECM with a spherical morphology. The stiff ECM also promoted increased stemness, hypoxia, and angiogenic potential in glioblastoma cells compared to the soft ECM. The softer ECM promoted cancer cell differentiation with fibroblast-like morphology and a good representation of classical GBM invasiveness. The 3D model with the stiffer ECM better mimicked the mesenchymal, proneural subtype of GBM that matched the gene expression data available in the Cancer Genome Atlas.[60] During the coculture, endothelial cells migrated toward the GBM cells in both stiff and soft ECM conditions. In the stiff ECM, the HUVECs were forming sprouting blood vessels toward GBM cells, whereas in the soft condition, the endothelial cells showed expansive growth toward the GBM.[60] The above study can be further expanded to other cancers to understand the impact of biophysical cues on tumor progression. Most of these studies on 3D bioprinted models for encapsulating the cancer cell and probing the ECM involve GelMA as the principal constituent, which lacks several other vital components such as glycoproteins and proteoglycans. Many of the ECM components lack in extrudability and the desired mechanical properties, limiting their applicatons in cancer research. Recently, porcine breast organ specific ECM was combined with alginate, GelMA, and collagen I to prepare the ECM-containing bioink that can be extruded without a support bath. The study provided means to isolate organ specific ECM, which can be further improved or modified with photocurable moieties to realize better *in vivo* specific biomimicry to recapitulate cancer cell−ECM interactions.[110] Incorporation of different cell types along with different biochemical gradients and cancer tissue-specific ECM can provide a better representation of the TME with the incorporation of different cell types to understand the cell−ECM interactions in tumor progression and invasion along with relevant drug development.

6. CONCLUSION AND FUTURE DIRECTIONS

PBs are widely adapted for tissue engineering applications, which can provide improved ways to establish large scale vascularized tumor models. Photopolymerization as a curing strategy provides a means to increase printability, resolution, and mechanical stability, while incorporating biochemical gradients in engineered 3D tumor models for recapitulating of TME complexity. Specifically, vat-based bioprinting approaches afford the incorporation of hollow channels, and inkjet-based printing of PBs provides high throughput spheroid formation capability. Extrusion-based bioprinting involving multicomponent ECM mimetic bioinks involving sacrificial bioprinting can help to recapitulate multicellular tissue interfaces to understand multicellular crosstalk involved in cancer metastasis. Combining strategies of high throughput spheroid formation along with microfluidic channel printability of vat-based techniques and facile multimaterial bioprintiability via extrusion bioprinting can help to recreate the TME efficiently for high throughput platforms. The combinatorial approaches can be explored to recreate different hallmarks and events of cancer, from primary tumor initiation to metastasis. Currently available PBs explored for cancer research need further improvement by incorporating physiologically relevant ECM mimetic photocurable ECM molecules such as elastin, glycoproteins, and glycosaminoglycans in appropriate ratios to effectively mimic the various tissue-specific cancers. Furthermore, biomimetic polymers and their physiologically relevant concentrations and ECM mimetic biomaterials to maintain the inter and intratumor heterogeneity can provide improved means to personalized drug response assessment, biomarkers identification, and disease biology modeling.

3D bioprinting techniques using PBs have gained significant attention in recent years to create complex hierarchical structures[134] due to the tunability of the bioinks for tissue engineering and disease modeling. Nevertheless, challenges such as far-UV-based curing, PI-induced cytotoxicity, oxygen-mediated inhibition of photopolymerization, long printing times, inability to establish spatiotemporal biochemical gradients, and lack of tissue-specific bioinks persist and must be overcome through continued research.[7] Several challenges, such as the visualization and cellular tracking in 3D, are yet to be resolved to gain better insights into cellular-level cross talks in 3D. Recent advances in PB-based bioprinting techniques, such as fast hydrogel stereolithography printing (FLOAT),[135] precured projection-based bioprinting,[136] and CAL,[137] can further reduce the time in printing large tissues for disease modeling. Strategies such as using visible light-responsive photopolymerization strategies with rapid curing and minimal oxygen-based inhibition cross-linking chemistries can further avoid cytotoxicity and genetic alterations during bioprinting.[30,138] Most of the current photopolymerization-based models are static cultures. Combing the microfluidics strategies with bioprinting techniques such as multimaterial steriolithography[139] can provide better control over the conventional microfluidics-based approach in creating vascularized tumor models containing gradients[65] with respect to cellular and physicochemical cues to mimic TME. These developments can offer better strategies to screen for advanced therapeutics such as adoptive cell transfer therapies. Emerging techniques such as four dimensional (4D) bioprinting are gaining importance due to the ability to induce shape change upon external stimulus to create complex structures such as vasculature and glandular[85] structures to recreate the dynamic tissue complexity, unlike the static 3D bioprinted models. Further, 4D bioprinting can reduce the time for creating complex geometries, such as hollow channel tubes, compared to conventional 3D printing approaches providing a better alternative to glandular tissue development for disease modeling.[75,140,141] Improving the bioink properties to incorporate cancer-specific ECM along with advancement in 3D bioprinting modalities with respect to resolution, reduced cost, printing speed, and better 3D analytic approaches can further advance the field of photopolymerization-based cancer research and offer unique opportunities to benefit cancer treatments. Application of artificial intelligence in 3D bioprinted cancer disease models can further provide opportunities for noninvasive early detection, accuracy, and platforms for incidence based, personalized treatment allocation through patient data mining approaches. Combination of microfluidics with PBs can provide approaches toward mechanically, biochemically tunable 3D bioprinted large scale constructs with perfusion to realize 3D bioprinted cancer on chip models. The potential of 3D-bioprinted cancer-on-a-chip platform for high-throughput/high-content screening in real time can be further improved by the inclusion of on-chip biosensors, thereby opening new avenues of discovery and accelerating the drug screening process.[43] These approaches can provide opportunities to integrate patient derived cancer cell culture for the long-term without affecting the tumor heterogeneity for accurate drug response relevant to *in vivo* conditions.

https://doi.org/10.1021/jacsau.3c00281
JACS Au 2023, 3, 2086−2106

AUTHOR INFORMATION

Corresponding Author

Kaushik Chatterjee − *Department of Materials Engineering Indian Institute of Science, Bangalore, Karnataka 560012, India;* orcid.org/0000-0002-7204-2926; Phone: +91-80-22933408; Email: kchatterjee@iisc.ac.in

Authors

Sriram Bharath Gugulothu − *Department of Materials Engineering Indian Institute of Science, Bangalore, Karnataka 560012, India*

Sonal Asthana − *Department of Materials Engineering Indian Institute of Science, Bangalore, Karnataka 560012, India; Department of Hepatobiliary and Multi-Organ Transplantation Surgery, Aster CMI Hospital, Bangalore 560024, India*

Shervanthi Homer-Vanniasinkam − *Department of Materials Engineering Indian Institute of Science, Bangalore, Karnataka 560012, India; Department of Mechanical Engineering and Division of Surgery, University College, London WC1E 7JE, U.K.*

Complete contact information is available at: https://pubs.acs.org/10.1021/jacsau.3c00281

Author Contributions

CRediT: **Sriram Bharath Gugulothu** conceptualization, data curation, formal analysis, writing-original draft; **Sonal Asthana** conceptualization, formal analysis, writing-review & editing; **Shervanthi Homer-Vanniasinkam** conceptualization, formal analysis, writing-review & editing; **Kaushik Chatterjee** conceptualization, formal analysis, writing-review & editing, supervision, project administration, funding acquisition.

Notes

The authors declare no competing financial interest.

ACKNOWLEDGMENTS

The authors thank the Science and Engineering Research Board (SERB), Government of India (IPA/2020/000025), for funding. S.B.G. is supported by the Prime Minister's Research Fellowship. S.B.G acknowledges Joel P. Joseph and Dr. Souvik Debnath for the insightful discussions. Organ images for the graphical abstract are reproduced with permission from freepik.com, and stock.adobe.com. 3D bioprinted construct image for Figure 3.b was created using biorender.com.

REFERENCES

(1) Barnes, J. M.; Przybyla, L.; Weaver, V. M. Tissue mechanics regulate brain development, homeostasis and disease. *Journal of cell science* **2017**, *130* (1), 71−82.

(2) Zeng, Z.; Wong, C. J.; Yang, L.; Ouardaoui, N.; Li, D.; Zhang, W.; Gu, S.; Zhang, Y.; Liu, Y.; Wang, X.; Fu, J.; Zhou, L.; Zhang, B.; Kim, S.; Yates, K. B.; Brown, M.; Freeman, G. J.; Uppaluri, R.; Manguso, R.; Liu, X. S. TISMO: syngeneic mouse tumor database to model tumor immunity and immunotherapy response. *Nucleic Acids Res.* **2022**, *50* (D1), D1391−d1397.

(3) Gómez-Cuadrado, L.; Tracey, N.; Ma, R.; Qian, B.; Brunton, V. G. Mouse models of metastasis: progress and prospects. *Disease models & mechanisms* **2017**, *10* (9), 1061−1074.

(4) Lwin, T. M.; Hoffman, R. M.; Bouvet, M. Advantages of patient-derived orthotopic mouse models and genetic reporters for developing fluorescence-guided surgery. *Journal of surgical oncology* **2018**, *118* (2), 253−264.

(5) Sajjad, H.; Imtiaz, S.; Noor, T.; Siddiqui, Y. H.; Sajjad, A.; Zia, M. Cancer models in preclinical research: A chronicle review of advancement in effective cancer research. *Animal Models and Experimental Medicine* **2021**, *4* (2), 87−103.

(6) Balachander, G. M.; Kotcherlakota, R.; Nayak, B.; Kedaria, D.; Rangarajan, A.; Chatterjee, K. 3D Tumor Models for Breast Cancer: Whither We Are and What We Need. *ACS Biomaterials Science & Engineering* **2021**, *7* (8), 3470−3486.

(7) Kang, Y.; Datta, P.; Shanmughapriya, S.; Ozbolat, I. T. 3D bioprinting of tumor models for cancer research. *ACS Applied Bio Materials* **2020**, *3* (9), 5552−5573.

(8) El Harane, S.; Zidi, B.; El Harane, N.; Krause, K.-H.; Matthes, T.; Preynat-Seauve, O. Cancer Spheroids and Organoids as Novel Tools for Research and Therapy: State of the Art and Challenges to Guide Precision Medicine. *Cells* **2023**, *12* (7), 1001.

(9) Unnikrishnan, K.; Thomas, L. V.; Ram Kumar, R. M. Advancement of Scaffold-Based 3D Cellular Models in Cancer Tissue Engineering: An Update. *Frontiers in Oncology* **2021**, *11*. DOI: 10.3389/fonc.2021.733652

(10) Wang, Y.; Gao, Y.; Pan, Y.; Zhou, D.; Liu, Y.; Yin, Y.; Yang, J.; Wang, Y.; Song, Y. Emerging trends in organ-on-a-chip systems for drug screening. *Acta Pharmaceutica Sinica B* **2023**, *13* (6), 2483−2509.

(11) Sontheimer-Phelps, A.; Hassell, B. A.; Ingber, D. E. Modelling cancer in microfluidic human organs-on-chips. *Nat. Rev. Cancer* **2019**, *19* (2), 65−81.

(12) Datta, P.; Dey, M.; Ataie, Z.; Unutmaz, D.; Ozbolat, I. T. 3D bioprinting for reconstituting the cancer microenvironment. *NPJ. precision oncology* **2020**, *4* (1), 1−13.

(13) Zadpoor, A. A.; Malda, J. Additive Manufacturing of Biomaterials, Tissues, and Organs. *Annals of Biomedical Engineering* **2017**, *45* (1), 1−11.

(14) Nilawar, S.; Chatterjee, K. Surface decoration of redox-modulating nanoceria on 3D-printed tissue scaffolds promotes stem cell osteogenesis and attenuates bacterial colonization. *Biomacromolecules* **2022**, *23* (1), 226−239.

(15) Mandrycky, C.; Wang, Z.; Kim, K.; Kim, D.-H. 3D bioprinting for engineering complex tissues. *Biotechnology advances* **2016**, *34* (4), 422−434.

(16) Kingsley, D. M.; Roberge, C. L.; Rudkouskaya, A.; Faulkner, D. E.; Barroso, M.; Intes, X.; Corr, D. T. Laser-based 3D bioprinting for spatial and size control of tumor spheroids and embryoid bodies. *Acta biomaterialia* **2019**, *95*, 357−370.

(17) Langer, E. M.; Allen-Petersen, B. L.; King, S. M.; Kendsersky, N. D.; Turnidge, M. A.; Kuziel, G. M.; Riggers, R.; Samatham, R.; Amery, T. S.; Jacques, S. L.; Sheppard, B. C.; Korkola, J. E.; Muschler, J. L.; Thibault, G.; Chang, Y. H.; Gray, J. W.; Presnell, S. C.; Nguyen, D. G.; Sears, R. C. Modeling Tumor Phenotypes In Vitro with Three-Dimensional Bioprinting. *Cell Reports* **2019**, *26* (3), 608−623.

(18) Li, J.; Parra-Cantu, C.; Wang, Z.; Zhang, Y. S. Improving bioprinted volumetric tumor microenvironments in vitro. *Trends in cancer* **2020**, *6* (9), 745−756.

(19) Ozbolat, I. T. *3D bioprinting: fundamentals, principles and applications*; Academic Press, 2016.

(20) Groll, J.; Burdick, J. A.; Cho, D.-W.; Derby, B.; Gelinsky, M.; Heilshorn, S. C.; Juengst, T.; Malda, J.; Mironov, V. A.; Nakayama, K.; et al. A definition of bioinks and their distinction from biomaterial inks. *Biofabrication* **2019**, *11* (1), 013001.

(21) GhavamiNejad, A.; Ashammakhi, N.; Wu, X. Y.; Khademhosseini, A. Crosslinking strategies for 3D bioprinting of polymeric hydrogels. *Small* **2020**, *16* (35), 2002931.

(22) Ji, Y.; Yang, Q.; Huang, G.; Shen, M.; Jian, Z.; Thoraval, M.-J.; Lian, Q.; Zhang, X.; Xu, F. Improved Resolution and Fidelity of Droplet-Based Bioprinting by Upward Ejection. *ACS Biomaterials Science & Engineering* **2019**, *5* (8), 4112−4121.

(23) Yang, Y.; Jia, Y.; Yang, Q.; Xu, F. Engineering bio-inks for 3D bioprinting cell mechanical microenvironment. *International Journal of Bioprinting* **2022**, *9* (1), 632 DOI: 10.18063/ijb.v9i1.632.

(24) Lee, M.; Rizzo, R.; Surman, F.; Zenobi-Wong, M. Guiding lights: tissue bioprinting using photoactivated materials. *Chem. Rev.* **2020**, *120* (19), 10950−11027.
(25) Ding, A.; Jeon, O.; Cleveland, D.; Gasvoda, K. L.; Wells, D.; Lee, S. J.; Alsberg, E. Jammed Micro-Flake Hydrogel for Four-Dimensional Living Cell Bioprinting. *Adv. Mater.* **2022**, *34* (15), 2109394.
(26) Ding, A.; Lee, S. J.; Ayyagari, S.; Tang, R.; Huynh, C. T.; Alsberg, E. 4D biofabrication via instantly generated graded hydrogel scaffolds. *Bioactive materials* **2022**, *7*, 324−332.
(27) Kumari, S.; Mondal, P.; Chatterjee, K. Digital light processing-based 3D bioprinting of κ-carrageenan hydrogels for engineering cell-loaded tissue scaffolds. *Carbohydr. Polym.* **2022**, *290*, 119508.
(28) He, Y.; Wang, F.; Wang, X.; Zhang, J.; Wang, D.; Huang, X. A photocurable hybrid chitosan/acrylamide bioink for DLP based 3D bioprinting. *Materials & Design* **2021**, *202*, 109588.
(29) Kim, M. H.; Lin, C.-C. Poly(ethylene glycol)-Norbornene as a Photoclick Bioink for Digital Light Processing 3D Bioprinting. *ACS Appl. Mater. Interfaces* **2023**, *15* (2), 2737−2746.
(30) Zheng, Z.; Eglin, D.; Alini, M.; Richards, G. R.; Qin, L.; Lai, Y. Visible light-induced 3D bioprinting technologies and corresponding bioink materials for tissue engineering: A review. *Engineering* **2021**, *7* (7), 966−978.
(31) Tromayer, M.; Dobos, A.; Gruber, P.; Ajami, A.; Dedic, R.; Ovsianikov, A.; Liska, R. A biocompatible diazosulfonate initiator for direct encapsulation of human stem cells via two-photon polymerization. *Polym. Chem.* **2018**, *9* (22), 3108−3117.
(32) Kumar, H.; Kim, K., Stereolithography 3D Bioprinting. In *3D Bioprinting: Principles and Protocols*; Crook, J. M., Ed.; Springer US: New York, 2020; pp 93−108.
(33) Shapira, A.; Noor, N.; Asulin, M.; Dvir, T. Stabilization strategies in extrusion-based 3D bioprinting for tissue engineering. *Applied Physics Reviews* **2018**, *5* (4), 041112.
(34) Duchamp, M.; Liu, T.; van Genderen, A. M.; Kappings, V.; Oklu, R.; Ellisen, L. W.; Zhang, Y. S. Sacrificial bioprinting of a mammary ductal carcinoma model. *Biotechnology journal* **2019**, *14* (10), 1700703.
(35) Albritton, J. L.; Miller, J. S. 3D bioprinting: improving in vitro models of metastasis with heterogeneous tumor microenvironments. *Disease models & mechanisms* **2017**, *10* (1), 3−14.
(36) Lim, K. S.; Galarraga, J. H.; Cui, X.; Lindberg, G. C.; Burdick, J. A.; Woodfield, T. B. Fundamentals and applications of photo-cross-linking in bioprinting. *Chem. Rev.* **2020**, *120* (19), 10662−10694.
(37) Zanon, M.; Baruffaldi, D.; Sangermano, M.; Pirri, C. F.; Frascella, F.; Chiappone, A. Visible light-induced crosslinking of unmodified gelatin with PEGDA for DLP-3D printable hydrogels. *Eur. Polym. J.* **2021**, *160*, 110813.
(38) Zhang, W.; Ye, W.; Yan, Y. Advances in photocrosslinkable materials for 3D bioprinting. *Adv. Eng. Mater.* **2022**, *24* (1), 2100663.
(39) Shukla, P.; Yeleswarapu, S.; Heinrich, M. A.; Prakash, J.; Pati, F. Mimicking tumor microenvironment by 3D bioprinting: 3D cancer modeling. *Biofabrication* **2022**, *14* (3), 032002.
(40) de Visser, K. E.; Joyce, J. A. The evolving tumor microenvironment: From cancer initiation to metastatic outgrowth. *Cancer Cell* **2023**, *41* (3), 374−403.
(41) Ma, L.; Li, Y.; Wu, Y.; Aazmi, A.; Zhang, B.; Zhou, H.; Yang, H. The construction of in vitro tumor models based on 3D bioprinting. *Bio-Design and Manufacturing* **2020**, *3*, 227−236.
(42) Sharma, R.; Restan Perez, M.; da Silva, V. A.; Thomsen, J.; Bhardwaj, L.; Andrade, T. A. M.; Alhussan, A.; Willerth, S. M. 3D bioprinting complex models of cancer. *Biomaterials Science* **2023**, *11* (10), 3414−3430.
(43) Monteiro, M. V.; Zhang, Y. S.; Gaspar, V. M.; Mano, J. F. 3D-bioprinted cancer-on-a-chip: Level-up organotypic in vitro models. *Trends Biotechnol.* **2022**, *40* (4), 432−447.
(44) Wei, R.; Liu, S.; Zhang, S.; Min, L.; Zhu, S. Cellular and extracellular components in tumor microenvironment and their application in early diagnosis of cancers. *Analytical Cellular Pathology* **2020**, *2020*, 1.
(45) Hoshiba, T. Decellularized extracellular matrix for cancer research. *Materials* **2019**, *12* (8), 1311.
(46) Pickup, M. W.; Mouw, J. K.; Weaver, V. M. The extracellular matrix modulates the hallmarks of cancer. *EMBO reports* **2014**, *15* (12), 1243−1253.
(47) Gkretsi, V.; Stylianopoulos, T. Cell adhesion and matrix stiffness: coordinating cancer cell invasion and metastasis. *Frontiers in oncology* **2018**, *8*, 145.
(48) Theocharis, A. D.; Karamanos, N. K. Proteoglycans remodeling in cancer: Underlying molecular mechanisms. *Matrix Biology* **2019**, *75*, 220−259.
(49) Balachander, G. M.; Talukdar, P. M.; Debnath, M.; Rangarajan, A.; Chatterjee, K. Inflammatory role of cancer-associated fibroblasts in invasive breast tumors revealed using a fibrous polymer scaffold. *ACS Appl. Mater. Interfaces* **2018**, *10* (40), 33814−33826.
(50) Qiu, S.-Q.; Waaijer, S. J.; Zwager, M. C.; de Vries, E. G.; van der Vegt, B.; Schröder, C. P. Tumor-associated macrophages in breast cancer: Innocent bystander or important player? *Cancer treatment reviews* **2018**, *70*, 178−189.
(51) Rafaeva, M.; Erler, J. T. Framing cancer progression: influence of the organ-and tumour-specific matrisome. *FEBS journal* **2020**, *287* (8), 1454−1477.
(52) Benwood, C.; Chrenek, J.; Kirsch, R. L.; Masri, N. Z.; Richards, H.; Teetzen, K.; Willerth, S. M. Natural biomaterials and their use as bioinks for printing tissues. *Bioengineering* **2021**, *8* (2), 27.
(53) Vanaei, S.; Parizi, M.S.; Vanaei, S.; Salemizadehparizi, F.; Vanaei, H.R. An overview on materials and techniques in 3D bioprinting toward biomedical application. *Engineered Regeneration* **2021**, *2*, 1−18.
(54) Bertassoni, L. E.; Cardoso, J. C.; Manoharan, V.; Cristino, A. L.; Bhise, N. S.; Araujo, W. A.; Zorlutuna, P.; Vrana, N. E.; Ghaemmaghami, A. M.; Dokmeci, M. R.; et al. Direct-write bioprinting of cell-laden methacrylated gelatin hydrogels. *Biofabrication* **2014**, *6* (2), 024105.
(55) Gillispie, G.; Prim, P.; Copus, J.; Fisher, J.; Mikos, A. G.; Yoo, J. J.; Atala, A.; Lee, S. J. Assessment methodologies for extrusion-based bioink printability. *Biofabrication* **2020**, *12* (2), 022003.
(56) Liu, T.; Liu, Q.; Anaya, I.; Huang, D.; Kong, W.; Mille, L. S.; Zhang, Y. S. Investigating lymphangiogenesis in a sacrificially bioprinted volumetric model of breast tumor tissue. *Methods* **2021**, *190*, 72−79.
(57) Surendran, V.; Rutledge, D.; Colmon, R.; Chandrasekaran, A. A novel tumor-immune microenvironment (TIME)-on-Chip mimics three dimensional neutrophil-tumor dynamics and neutrophil extracellular traps (NETs)-mediated collective tumor invasion. *Biofabrication* **2021**, *13* (3), 035029.
(58) Bhise, N. S.; Manoharan, V.; Massa, S.; Tamayol, A.; Ghaderi, M.; Miscuglio, M.; Lang, Q.; Zhang, Y. S.; Shin, S. R.; Calzone, G.; et al. A liver-on-a-chip platform with bioprinted hepatic spheroids. *Biofabrication* **2016**, *8* (1), 014101.
(59) Grigoryan, B.; Paulsen, S. J.; Corbett, D. C.; Sazer, D. W.; Fortin, C. L.; Zaita, A. J.; Greenfield, P. T.; Calafat, N. J.; Gounley, J. P.; Ta, A. H.; et al. Multivascular networks and functional intravascular topologies within biocompatible hydrogels. *Science* **2019**, *364* (6439), 458−464.
(60) Tang, M.; Tiwari, S. K.; Agrawal, K.; Tan, M.; Dang, J.; Tam, T.; Tian, J.; Wan, X.; Schimelman, J.; You, S.; et al. Rapid 3D bioprinting of glioblastoma model mimicking native biophysical heterogeneity. *Small* **2021**, *17* (15), 2006050.
(61) Ng, W. L.; Lee, J. M.; Zhou, M.; Chen, Y.-W.; Lee, K.-X. A.; Yeong, W. Y.; Shen, Y.-F. Vat polymerization-based bioprinting—Process, materials, applications and regulatory challenges. *Biofabrication* **2020**, *12* (2), 022001.
(62) Li, Y.; Mao, Q.; Xu, K.; Yang, H.; Huang, Y.; Yin, J. Photopolymerization Bioprinting with a Dynamic Support Bath. *Additive Manufacturing* **2023**, *69*, 103533.
(63) Regehly, M.; Garmshausen, Y.; Reuter, M.; König, N. F.; Israel, E.; Kelly, D. P.; Chou, C.-Y.; Koch, K.; Asfari, B.; Hecht, S.

https://doi.org/10.1021/jacsau.3c00281
JACS Au 2023, 3, 2086−2106

Xolography for linear volumetric 3D printing. *Nature* **2020**, *588* (7839), 620−624.
(64) Tavares-Negrete, J. A.; Babayigit, C.; Najafikoshnoo, S.; Lee, S. W.; Boyraz, O.; Esfandyarpour, R. A Novel 3D-Bioprinting Technology of Orderly Extruded Multi-Materials via Photopolymerization. *Advanced Materials Technologies* **2023**, *8* (12), 2201926.
(65) Wang, M.; Li, W.; Mille, L. S.; Ching, T.; Luo, Z.; Tang, G.; Garciamendez, C. E.; Lesha, A.; Hashimoto, M.; Zhang, Y. S. Digital Light Processing Based Bioprinting with Composable Gradients. *Adv. Mater.* **2022**, *34* (1), 2107038.
(66) Gudapati, H.; Dey, M.; Ozbolat, I. A comprehensive review on droplet-based bioprinting: Past, present and future. *Biomaterials* **2016**, *102*, 20−42.
(67) Banerjee, D.; Singh, Y. P.; Datta, P.; Ozbolat, V.; O'Donnell, A.; Yeo, M.; Ozbolat, I. T. Strategies for 3D bioprinting of spheroids: A comprehensive review. *Biomaterials* **2022**, *291*, 121881.
(68) Hakobyan, D.; Médina, C.; Dusserre, N.; Stachowicz, M.-L.; Handschin, C.; Fricain, J.-C.; Guillermet-Guibert, J.; Oliveira, H. Laser-assisted 3D bioprinting of exocrine pancreas spheroid models for cancer initiation study. *Biofabrication* **2020**, *12* (3), 035001.
(69) Chen, K.; Jiang, E.; Wei, X.; Xia, Y.; Wu, Z.; Gong, Z.; Shang, Z.; Guo, S. The acoustic droplet printing of functional tumor microenvironments. *Lab Chip* **2021**, *21* (8), 1604−1612.
(70) Lee, Y.; Park, J. A.; Tuladhar, T.; Jung, S. Sonochemical Degradation Of Gelatin Methacryloyl To Control Viscoelasticity for Inkjet Bioprinting. *Macromol. Biosci.* **2023**, *23*, 2200509.
(71) Joshi, A.; Choudhury, S.; Gugulothu, S. B.; Visweswariah, S. S.; Chatterjee, K. Strategies to Promote Vascularization in 3D Printed Tissue Scaffolds: Trends and Challenges. *Biomacromolecules* **2022**, *23* (7), 2730−2751.
(72) Iervolino, F.; Belgio, B.; Bonessa, A.; Potere, F.; Suriano, R.; Boschetti, F.; Mantero, S.; Levi, M. Versatile and non-cytotoxic GelMA-xanthan gum biomaterial ink for extrusion-based 3D bioprinting. *Bioprinting* **2023**, *31*, No. e00269.
(73) Rastin, H.; Ormsby, R. T.; Atkins, G. J.; Losic, D. 3D bioprinting of methylcellulose/gelatin-methacryloyl (MC/GelMA) bioink with high shape integrity. *ACS Applied Bio Materials* **2020**, *3* (3), 1815−1826.
(74) You, S.; Xiang, Y.; Hwang, H. H.; Berry, D. B.; Kiratitanaporn, W.; Guan, J.; Yao, E.; Tang, M.; Zhong, Z.; Ma, X.; et al. High cell density and high-resolution 3D bioprinting for fabricating vascularized tissues. *Science Advances* **2023**, *9* (8), No. eade7923.
(75) Gugulothu, S. B.; Chatterjee, K. Visible Light-Based 4D-Bioprinted Tissue Scaffold. *ACS Macro Lett.* **2023**, *12*, 494−502.
(76) Xu, H.; Casillas, J.; Krishnamoorthy, S.; Xu, C. Effects of Irgacure 2959 and lithium phenyl-2,4,6-trimethylbenzoylphosphinate on cell viability, physical properties, and microstructure in 3D bioprinting of vascular-like constructs. *Biomedical Materials* **2020**, *15* (5), 055021.
(77) He, N.; Wang, X.; Shi, L.; Li, J.; Mo, L.; Chen, F.; Huang, Y.; Liu, H.; Zhu, X.; Zhu, W.; et al. Photoinhibiting via simultaneous photoabsorption and free-radical reaction for high-fidelity light-based bioprinting. *Nat. Commun.* **2023**, *14* (1), 1−15.
(78) Lim, K. S.; Levato, R.; Costa, P. F.; Castilho, M. D.; Alcala-Orozco, C. R.; van Dorenmalen, K. M. A.; Melchels, F. P. W.; Gawlitta, D.; Hooper, G. J.; Malda, J.; Woodfield, T. B. F. Bio-resin for high resolution lithography-based biofabrication of complex cell-laden constructs. *Biofabrication* **2018**, *10* (3), 034101.
(79) Levato, R.; Lim, K. S.; Li, W.; Asua, A. U.; Peña, L. B.; Wang, M.; Falandt, M.; Bernal, P. N.; Gawlitta, D.; Zhang, Y. S.; et al. High-resolution lithographic biofabrication of hydrogels with complex microchannels from low-temperature-soluble gelatin bioresins. *Materials Today Bio* **2021**, *12*, 100162.
(80) Shanjani, Y.; Pan, C.; Elomaa, L.; Yang, Y. A novel bioprinting method and system for forming hybrid tissue engineering constructs. *Biofabrication* **2015**, *7* (4), 045008.
(81) Rajput, M.; Mondal, P.; Yadav, P.; Chatterjee, K. Light-based 3D bioprinting of bone tissue scaffolds with tunable mechanical properties and architecture from photocurable silk fibroin. *Int. J. Biol. Macromol.* **2022**, *202*, 644−656.
(82) He, J.; Sun, Y.; Gao, Q.; He, C.; Yao, K.; Wang, T.; Xie, M.; Yu, K.; Nie, J.; Chen, Y.; et al. Gelatin Methacryloyl Hydrogel, from Standardization, Performance, to Biomedical Application. *Adv. Healthcare Mater.* **2023**, 2300395.
(83) Soman, P.; Kelber, J. A.; Lee, J. W.; Wright, T. N.; Vecchio, K. S.; Klemke, R. L.; Chen, S. Cancer cell migration within 3D layer-by-layer microfabricated photocrosslinked PEG scaffolds with tunable stiffness. *Biomaterials* **2012**, *33* (29), 7064−7070.
(84) Huang, T. Q.; Qu, X.; Liu, J.; Chen, S. 3D printing of biomimetic microstructures for cancer cell migration. *Biomed. Microdevices* **2014**, *16* (1), 127−132.
(85) Kwag, H. R.; Serbo, J. V.; Korangath, P.; Sukumar, S.; Romer, L. H.; Gracias, D. H. A self-folding hydrogel in vitro model for ductal carcinoma. *Tissue Engineering Part C: Methods* **2016**, *22* (4), 398−407.
(86) Piluso, S.; Skvortsov, G. A.; Altunbek, M.; Afghah, F.; Khani, N.; Koç, B.; Patterson, J. 3D bioprinting of molecularly engineered PEG-based hydrogels utilizing gelatin fragments. *Biofabrication* **2021**, *13* (4), 045008.
(87) Ashammakhi, N.; Ahadian, S.; Xu, C.; Montazerian, H.; Ko, H.; Nasiri, R.; Barros, N.; Khademhosseini, A. Bioinks and bioprinting technologies to make heterogeneous and biomimetic tissue constructs. *Materials Today Bio* **2019**, *1*, 100008.
(88) Tytgat, L.; Dobos, A.; Markovic, M.; Van Damme, L.; Van Hoorick, J.; Bray, F.; Thienpont, H.; Ottevaere, H.; Dubruel, P.; Ovsianikov, A.; et al. High-resolution 3D bioprinting of photo-crosslinkable recombinant collagen to serve tissue engineering applications. *Biomacromolecules* **2020**, *21* (10), 3997−4007.
(89) Visscher, D. O.; Lee, H.; van Zuijlen, P. P.; Helder, M. N.; Atala, A.; Yoo, J. J.; Lee, S. J. A photo-crosslinkable cartilage-derived extracellular matrix bioink for auricular cartilage tissue engineering. *Acta biomaterialia* **2021**, *121*, 193−203.
(90) Indrakumar, S.; Joshi, A.; Dash, T. K.; Mishra, V.; Tandon, B.; Chatterjee, K. Photopolymerized silk fibroin gel for advanced burn wound care. *Int. J. Biol. Macromol.* **2023**, *233*, 123569.
(91) Donnelly, P. E.; Chen, T.; Finch, A.; Brial, C.; Maher, S. A.; Torzilli, P. A. Photocrosslinked tyramine-substituted hyaluronate hydrogels with tunable mechanical properties improve immediate tissue-hydrogel interfacial strength in articular cartilage. *Journal of Biomaterials science, Polymer edition* **2017**, *28* (6), 582−600.
(92) Hu, J.; Hou, Y.; Park, H.; Choi, B.; Hou, S.; Chung, A.; Lee, M. Visible light crosslinkable chitosan hydrogels for tissue engineering. *Acta biomaterialia* **2012**, *8* (5), 1730−1738.
(93) Wloka, T.; Gottschaldt, M.; Schubert, U. S. From Light to Structure: Photo Initiators for Radical Two-Photon Polymerization. *Chem. Eur. J.* **2022**, *28* (32), No. e202104191.
(94) Bonardi, A.; Dumur, F.; Grant, T.; Noirbent, G.; Gigmes, D.; Lessard, B.; Fouassier, J.-P.; Lalevée, J. High performance near-infrared (NIR) photoinitiating systems operating under low light intensity and in the presence of oxygen. *Macromolecules* **2018**, *51* (4), 1314−1324.
(95) Lim, K. S.; Schon, B. S.; Mekhileri, N. V.; Brown, G. C. J.; Chia, C. M.; Prabakar, S.; Hooper, G. J.; Woodfield, T. B. F. New Visible-Light Photoinitiating System for Improved Print Fidelity in Gelatin-Based Bioinks. *ACS Biomaterials Science & Engineering* **2016**, *2* (10), 1752−1762.
(96) Zhang, Q.; Bei, H.-P.; Zhao, M.; Dong, Z.; Zhao, X. Shedding light on 3D printing: Printing photo-crosslinkable constructs for tissue engineering. *Biomaterials* **2022**, *286*, 121566.
(97) Nayak, B.; Balachander, G. M.; Manjunath, S.; Rangarajan, A.; Chatterjee, K. Tissue mimetic 3D scaffold for breast tumor-derived organoid culture toward personalized chemotherapy. *Colloids Surf., B* **2019**, *180*, 334−343.
(98) Leiva, M. C.; Garre, E.; Gustafsson, A.; Svanström, A.; Bogestål, Y.; Håkansson, J.; Ståhlberg, A.; Landberg, G. Breast cancer patient-derived scaffolds as a tool to monitor chemotherapy responses in human tumor microenvironments. *Journal of cellular physiology* **2021**, *236* (6), 4709−4724.

https://doi.org/10.1021/jacsau.3c00281
JACS Au 2023, 3, 2086−2106

(99) Heinrich, M. A.; Bansal, R.; Lammers, T.; Zhang, Y. S.; Michel Schiffelers, R.; Prakash, J. 3D-bioprinted mini-brain: a glioblastoma model to study cellular interactions and therapeutics. *Advanced materials* **2019**, *31* (14), 1806590.
(100) Tang, M.; Xie, Q.; Gimple, R. C.; Zhong, Z.; Tam, T.; Tian, J.; Kidwell, R. L.; Wu, Q.; Prager, B. C.; Qiu, Z.; et al. Three-dimensional bioprinted glioblastoma microenvironments model cellular dependencies and immune interactions. *Cell research* **2020**, *30* (10), 833−853.
(101) Miri, A. K.; Nieto, D.; Iglesias, L.; Goodarzi Hosseinabadi, H.; Maharjan, S.; Ruiz-Esparza, G. U.; Khoshakhlagh, P.; Manbachi, A.; Dokmeci, M. R.; Chen, S.; et al. Microfluidics-enabled multimaterial maskless stereolithographic bioprinting. *Adv. Mater.* **2018**, *30* (27), 1800242.
(102) Zhou, X.; Zhu, W.; Nowicki, M.; Miao, S.; Cui, H.; Holmes, B.; Glazer, R. I.; Zhang, L. G. 3D bioprinting a cell-laden bone matrix for breast cancer metastasis study. *ACS Appl. Mater. Interfaces* **2016**, *8* (44), 30017−30026.
(103) Cui, H.; Esworthy, T.; Zhou, X.; Hann, S. Y.; Glazer, R. I.; Li, R.; Zhang, L. G. Engineering a novel 3D printed vascularized tissue model for investigating breast cancer metastasis to bone. *Adv. Healthcare Mater.* **2020**, *9* (15), 1900924.
(104) Xie, M.; Gao, Q.; Qiu, J.; Fu, J.; Chen, Z.; He, Y. 3D biofabrication of microfiber-laden minispheroids: a facile 3D cell co-culturing system. *Biomaterials science* **2020**, *8* (1), 109−117.
(105) Shao, L.; Gao, Q.; Xie, C.; Fu, J.; Xiang, M.; He, Y. Directly coaxial 3D bioprinting of large-scale vascularized tissue constructs. *Biofabrication* **2020**, *12* (3), 035014.
(106) Ling, K.; Huang, G.; Liu, J.; Zhang, X.; Ma, Y.; Lu, T.; Xu, F. Bioprinting-based high-throughput fabrication of three-dimensional MCF-7 human breast cancer cellular spheroids. *Engineering* **2015**, *1* (2), 269−274.
(107) Yang, W.; Cai, S.; Yuan, Z.; Lai, Y.; Yu, H.; Wang, Y.; Liu, L. Mask-free generation of multicellular 3D heterospheroids array for high-throughput combinatorial anti-cancer drug screening. *Materials & Design* **2019**, *183*, 108182.
(108) Wei, X.; Huang, B.; Chen, K.; Fan, Z.; Wang, L.; Xu, M. Dot extrusion bioprinting of spatially controlled heterogenous tumor models. *Materials & Design* **2022**, *223*, 111152.
(109) Cao, X.; Ashfaq, R.; Cheng, F.; Maharjan, S.; Li, J.; Ying, G.; Hassan, S.; Xiao, H.; Yue, K.; Zhang, Y. S. A tumor-on-a-chip system with bioprinted blood and lymphatic vessel pair. *Adv. Funct. Mater.* **2019**, *29* (31), 1807173.
(110) Blanco-Fernandez, B.; Rey-Vinolas, S.; Bagci, G.; Rubi-Sans, G.; Otero, J.; Navajas, D.; Perez-Amodio, S.; Engel, E. Bioprinting Decellularized Breast Tissue for the Development of Three-Dimensional Breast Cancer Models. *ACS Appl. Mater. Interfaces* **2022**, *14* (26), 29467−29482.
(111) Zhu, W.; Qu, X.; Zhu, J.; Ma, X.; Patel, S.; Liu, J.; Wang, P.; Lai, C. S. E.; Gou, M.; Xu, Y.; et al. Direct 3D bioprinting of prevascularized tissue constructs with complex microarchitecture. *Biomaterials* **2017**, *124*, 106−115.
(112) Miao, T.; Chen, K.; Wei, X.; Huang, B.; Qian, Y.; Wang, L.; Xu, M. High-throughput fabrication of cell spheroids with 3D acoustic assembly devices. *Int. J. Bioprint* **2023**, *9* (4), 733.
(113) Meng, F.; Meyer, C. M.; Joung, D.; Vallera, D. A.; McAlpine, M. C.; Panoskaltsis-Mortari, A. 3D bioprinted in vitro metastatic models via reconstruction of tumor microenvironments. *Adv. Mater.* **2019**, *31* (10), 1806899.
(114) Mei, Y.; Wu, D.; Berg, J.; Tolksdorf, B.; Roehrs, V.; Kurreck, A.; Hiller, T.; Kurreck, J. Generation of a Perfusable 3D Lung Cancer Model by Digital Light Processing. *International Journal of Molecular Sciences* **2023**, *24* (7), 6071.
(115) Huang, B.; Wei, X.; Chen, K.; Wang, L.; Xu, M. Bioprinting of hydrogel beads to engineer pancreatic tumor-stroma microtissues for drug screening. *Int. J. Bioprint* **2023**, *9* (3), 676.
(116) Zhang, Z.; Zhou, L.; Xie, N.; Nice, E. C.; Zhang, T.; Cui, Y.; Huang, C. Overcoming cancer therapeutic bottleneck by drug repurposing. *Signal transduction and targeted therapy* **2020**, *5* (1), 1−25.
(117) Seyfried, T. N.; Huysentruyt, L. C. On the origin of cancer metastasis. *Crit Rev. Oncog* **2013**, *18* (1−2), 43−73.
(118) Day, C.-P.; Merlino, G.; Van Dyke, T. Preclinical mouse cancer models: a maze of opportunities and challenges. *Cell* **2015**, *163* (1), 39−53.
(119) Patel, N. R.; Aryasomayajula, B.; Abouzeid, A. H.; Torchilin, V. P. Cancer cell spheroids for screening of chemotherapeutics and drug-delivery systems. *Therapeutic delivery* **2015**, *6* (4), 509−520.
(120) Augustine, R.; Kalva, S. N.; Ahmad, R.; Zahid, A. A.; Hasan, S.; Nayeem, A.; McClements, L.; Hasan, A. 3D Bioprinted cancer models: Revolutionizing personalized cancer therapy. *Translational Oncology* **2021**, *14* (4), 101015.
(121) Jung, M.; Ghamrawi, S.; Du, E. Y.; Gooding, J. J.; Kavallaris, M. Advances in 3D bioprinting for cancer biology and precision medicine: From matrix design to application. *Adv. Healthcare Mater.* **2022**, *11* (24), 2200690.
(122) Hapach, L. A.; Mosier, J. A.; Wang, W.; Reinhart-King, C. A. Engineered models to parse apart the metastatic cascade. *npj Precision Oncology* **2019**, *3* (1), 20.
(123) Fares, J.; Fares, M. Y.; Khachfe, H. H.; Salhab, H. A.; Fares, Y. Molecular principles of metastasis: a hallmark of cancer revisited. *Signal transduction and targeted therapy* **2020**, *5* (1), 1−17.
(124) Macedo, F.; Ladeira, K.; Pinho, F.; Saraiva, N.; Bonito, N.; Pinto, L.; Goncalves, F. Bone Metastases: An Overview. *Oncol Rev.* **2017**, *11* (1), 321.
(125) Huang, Q.; Hu, X.; He, W.; Zhao, Y.; Hao, S.; Wu, Q.; Li, S.; Zhang, S.; Shi, M. Fluid shear stress and tumor metastasis. *American journal of cancer research* **2018**, *8* (5), 763.
(126) Ma, Y.-H. V.; Middleton, K.; You, L.; Sun, Y. A review of microfluidic approaches for investigating cancer extravasation during metastasis. *Microsystems Nanoengineering* **2018**, *4* (1), 1−13.
(127) Regmi, S.; Poudel, C.; Adhikari, R.; Luo, K. Q. Applications of Microfluidics and Organ-on-a-Chip in Cancer Research. *Biosensors* **2022**, *12* (7), 459.
(128) Nishida-Aoki, N.; Gujral, T. S. Emerging approaches to study cell-cell interactions in tumor microenvironment. *Oncotarget* **2019**, *10* (7), 785.
(129) Ning, L.; Shim, J.; Tomov, M. L.; Liu, R.; Mehta, R.; Mingee, A.; Hwang, B.; Jin, L.; Mantalaris, A.; Xu, C.; Mahmoudi, M.; Goldsmith, K. C.; Serpooshan, V. A 3D Bioprinted in vitro Model of Neuroblastoma Recapitulates Dynamic Tumor-Endothelial Cell Interactions Contributing to Solid Tumor Aggressive Behavior. *Advanced Science* **2022**, *9* (23), 2200244.
(130) Joseph, J. P.; Gugulothu, S. B.; Nandi, D.; Chatterjee, K. Mechanical Properties Affect Primary T Cell Activation in 3D Bioprinted Hydrogels. *ACS Macro Lett.* **2023**, 1085−1093.
(131) He, X.; Lee, B.; Jiang, Y. Cell-ECM interactions in tumor invasion. *Systems Biology of Tumor Microenvironment* **2016**, *936*, 73−91.
(132) Winkler, J.; Abisoye-Ogunniyan, A.; Metcalf, K. J.; Werb, Z. Concepts of extracellular matrix remodelling in tumour progression and metastasis. *Nat. Commun.* **2020**, *11* (1), 1−19.
(133) Li, H.; Dai, J.; Wang, Z.; Zheng, H.; Li, W.; Wang, M.; Cheng, F. Digital light processing (DLP)-based (bio)printing strategies for tissue modeling and regeneration. *Aggregate* **2023**, *4* (2), No. e270.
(134) Joshi, A.; Kaur, T.; Joshi, A.; Gugulothu, S. B.; Choudhury, S.; Singh, N. Light-Mediated 3D Printing of Micro-Pyramid-Decorated Tailorable Wound Dressings with Endogenous Growth Factor Sequestration for Improved Wound Healing. *ACS Appl. Mater. Interfaces* **2023**, *15* (1), 327−337.
(135) Anandakrishnan, N.; Ye, H.; Guo, Z.; Chen, Z.; Mentkowski, K. I.; Lang, J. K.; Rajabian, N.; Andreadis, S. T.; Ma, Z.; Spernyak, J. A.; et al. Fast stereolithography printing of large-scale biocompatible hydrogel models. *Adv. Healthcare Mater.* **2021**, *10* (10), 2002103.
(136) Li, Y.; Mao, Q.; Li, X.; Yin, J.; Wang, Y.; Fu, J.; Huang, Y. High-fidelity and high-efficiency additive manufacturing using tunable

https://doi.org/10.1021/jacsau.3c00281
JACS Au 2023, 3, 2086−2106

pre-curing digital light processing. *Additive Manufacturing* **2019**, *30*, 100889.
(137) Kelly, B. E.; Bhattacharya, I.; Heidari, H.; Shusteff, M.; Spadaccini, C. M.; Taylor, H. K. Volumetric additive manufacturing via tomographic reconstruction. *Science* **2019**, *363* (6431), 1075−1079.
(138) Lim, K. S.; Klotz, B. J.; Lindberg, G. C.; Melchels, F. P.; Hooper, G. J.; Malda, J.; Gawlitta, D.; Woodfield, T. B. Visible light cross-linking of gelatin hydrogels offers an enhanced cell microenvironment with improved light penetration depth. *Macromol. Biosci.* **2019**, *19* (6), 1900098.
(139) Grigoryan, B.; Sazer, D. W.; Avila, A.; Albritton, J. L.; Padhye, A.; Ta, A. H.; Greenfield, P. T.; Gibbons, D. L.; Miller, J. S. Development, characterization, and applications of multi-material stereolithography bioprinting. *Sci. Rep.* **2021**, *11* (1), 1−13.
(140) Kim, S. H.; Seo, Y. B.; Yeon, Y. K.; Lee, Y. J.; Park, H. S.; Sultan, M. T.; Lee, J. M.; Lee, J. S.; Lee, O. J.; Hong, H.; et al. 4D-bioprinted silk hydrogels for tissue engineering. *Biomaterials* **2020**, *260*, 120281.
(141) Mandal, A.; Chatterjee, K. Emerging Trends in Humidity-responsive 4D Bioprinting. *Chemical Engineering Journal* **2023**, *455*, 140550.

https://doi.org/10.1021/jacsau.3c00281
JACS Au 2023, 3, 2086−2106